J. Chem. Thermodynamics 217 (2026) 107675

Contents lists available at ScienceDirect

The Journal of Chemical Thermodynamics

journal homepage: www.journals.elsevier.com/the-journal-of-chemical-thermodynamics

Solubility measurements of carbon dioxide and nitrous oxide in an aqueous mixture of 2-dimethylaminoethanol and N-methyl-1,3-propanediamine

Juan D. Arroyave [a], Alejandro Moreau [a], Xavier Paredes [a], Fredy Vélez [a], J.P. Martin Trusler [b], M. Carmen Martín [a,*]

[a] TermoCal Research Group, Research Institute on Bioeconomy, University of Valladolid, Valladolid, Spain
[b] Department of Chemical Engineering, Imperial College London, London, UK

ARTICLE INFO

Keywords:
CO_2 capture
Amine blends
DMAE
MAPA
Vapour-liquid equilibrium
Solubility

ABSTRACT

Aqueous monoethanolamine (MEA) is a mature post-combustion CO_2 capture technology, but it faces significant drawbacks including corrosivity, high regeneration energy (~4 GJ/t-CO_2), and reactivity with contaminants. This study investigates an aqueous blend of 2-Dimethylaminoethanol (DMAE, 30% wt.) and N-Methyl-1,3-propanediamine (MAPA, 10% wt.) as an alternative solvent to capture CO_2. Given the scarcity of Vapour-Liquid Equilibrium (VLE) data for such amine blends, this research aims to expand the thermodynamic understanding of this specific aqueous DMAE + MAPA system. We thoroughly investigate its VLE with CO_2 and N_2O across temperatures between (313.15–393.15) K. The physical solubility of CO_2 was determined using the N_2O/CO_2 analogy. N_2O solubility measurements were conducted in a monobloc equilibrium cell from 1 to 5 MPa. The expanded relative uncertainty of the N_2O solubility, expressed in molality, was estimated to be 0.8% ($k = 2$). Henry's constants were derived using Krichevsky-Ilinskaya analysis and CO_2 solubility was determined using a static-isochoric Van Ness-type apparatus over 313.15–363.15 K and up to 7 MPa with a relative uncertainty of $u_r(\alpha_{exp}) = (0.3–5)$ %. Finally, speciation profiles and the heat of CO_2 absorption were predicted using established thermodynamic models optimized for this system.

1. Introduction

Aqueous monoethanolamine (MEA) scrubbing is a well-established post-combustion CO_2 capture technology, widely deployed due to the ease of solvent production, high CO_2 reactivity, strong alkalinity, and acceptable absorption capacity, even at low CO_2 concentrations [1]. However, significant operational costs are associated with this technology, stemming from its corrosive behaviour, high maintenance requirements, poor thermal stability, substantial regeneration energy penalty (3.99 GJ/t-CO_2), and reactivity with contaminants such as NO_x and SO_2, which accelerate degradation and reduce cyclic capacity [2].

Recent research has increasingly focused on the selection of alternative chemical and physical solvents to mitigate the drawbacks related to conventional amines, such as MEA. Furthermore, the blending of different kind of amines, based on their respective physical and chemical properties, has been explored to optimize CO_2 capture by enhancing both absorption and regeneration performance [3]. For instance, 2-dimethylaminoethanol (DMAE), a tertiary amine, has been widely studied for its reaction kinetics and potential advantages over primary amines, such as 1-amino-2-propanol (1A2P) and 3-amino-1-propanol (3A1P), as well as tertiary amines like *N*-methyldiethanolamine (MDEA) or diethyl-monoethanolamine (DEMEA) [4]. DMAE generally exhibits an enhanced reaction rate in CO_2 hydration due to its basic catalytic mechanism, which facilitates the nucleophilic attack of the amine group on the electrophilic carbon of CO_2. Moreover, the aqueous blend of DMAE with MEA demonstrates the potential to significantly augment the cyclic capacity of the solvent by nearly 100% compared to other tertiary and sterically hindered amines, including N,N-diethylethanolamine (DEEA) and 2-amino-2-methyl-1-propanol (AMP) [5]. Delavari et al. [6] measured the solubility of CO_2 in aqueous solutions containing DMAE (40% wt. or 30% wt.) and a secondary amine such as 2-(ethylamine)ethanol (EAE) (5% wt.) at temperatures ranging from 313.15 to 358.15 K and pressures from 6.5 to 236 kPa. In this case, DMAE allows a reduction in the absorption heat by approximately ~50 kJ/mol-CO_2 at loadings close to the solubility limit.

When initially selecting a CO_2 absorption solvent, three key

* Corresponding author.
E-mail address: mcarmen.martin@uva.es (M.C. Martín).

https://doi.org/10.1016/j.jct.2026.107675
Received 16 December 2025; Received in revised form 24 March 2026; Accepted 29 March 2026
Available online 30 March 2026

properties should be evaluated: CO_2 solubility, energy requirement for solvent regeneration, and kinetics of the amine reaction with CO_2 [7]. While DMAE is a suitable amine that exhibits high performance in these properties, its reactivity with CO_2 in aqueous media could be further improved by mixing with an alkyl amine with multiple amino groups. For example, MAPA, a diamine, is known to enhance CO_2 reactivity by nearly 15 times compared to MEA [8]. Choi et al. [9] investigated various blends of MDEA (20% wt.) with different activators (10% wt.), including MAPA, diethylenetriamine (DETA), triethylenetetramine (TETA), and tetraethylenepentamine (TEPA), to evaluate their absorption capacity, reaction rate, and heat of absorption. The study revealed that MAPA significantly enhanced the mass transfer coefficient, reaching a value of 3.4 $kmol{\cdot}m^{-2}{\cdot}s^{-1}{\cdot}kPa^{-1}$. This represents an eightfold improvement compared to MDEA or MEA, the reference amines. The enhanced reactivity of MAPA, likely due to its two amino groups, is believed to contribute to this significant increase in CO_2 absorption performance. García et al. [10] investigated the system N,N-diethylethanolamine (DEEA, 3 M) + MAPA (2 M) at temperatures ranging from 298 to 353 K, partial pressures of CO_2 between 10 and 15 kPa, and CO_2 loadings from 0 to 1.76 mol-CO_2/mol-amine. Their results demonstrated that this DEEA-MAPA blend exhibits higher mass transfer coefficient and kinetic performance than the conventional MEA-based system at 5 M concentration. Kruszczak and Kierzkowska-Pawlak [11] conducted a comparative study on the absorption velocity of aqueous amine blends containing DEEA and various activators, including AMP, 2-amino-2-methyl-1,3-propanediol (AMPD), and MAPA. The study was conducted at a total amine concentration of 2 M and temperatures ranging from 303 to 333 K. The results demonstrated that MAPA is the most effective activator among the tested options, making it a promising polyamine for various CO_2 capture applications [12].

It is important to select the quantity of each amine, particularly in cases where transport properties may be compromised. For instance, Monteiro et al. [13] investigated the kinetics of CO_2 absorption in aqueous blends of DEEA (1–5 M) and MAPA (1–2 M), as well as the density, viscosity, and solubility of N_2O. Their findings revealed a strong correlation between the total amine concentration in water and the viscosity of the solution. At 20 °C and a total amine concentration of 6 M, the viscosity reached a value of up to 20 mPa·s. Knuutila and Nannestad [14] characterized the DEEA-MAPA system by measuring the CO_2 heat of absorption at various temperatures (40 °C, 80 °C, and 120 °C). Their findings highlighted the importance of maintaining a lower MAPA concentration than the tertiary amine concentration. This condition is crucial for minimizing the absorption heat, particularly at low CO_2 loadings below 0.5 mol-CO_2/mol-amine and for preventing a decrease in cyclic capacity [15].

Specifically, for blended amine systems containing DMAE and MAPA, limited VLE data are available, despite their significant advantages in terms of heat of absorption, kinetics, and overall solution capacity [16]. Brúder et al. [17] conducted pilot-scale experiments in a plant capable of processing 150 Nm^3/h of flue gas, achieving a capture efficiency of 13 kg CO_2/h. Their results demonstrated the technical feasibility of using this blend and highlighted its reduced environmental impact compared to other amine mixtures based on AMP + Piperazine (PZ) or even MEA. Rahimi et al. [18] conducted equilibrium measurements of CO_2 absorption in various amine blends, including DMAE + MAPA, DMAE + AEEA, MDEA + MAPA, MDEA + AEEA, DEAE + MAPA, and DEAE + AEEA and Zoghi et al. [19] measured the solubility of CO_2 in a mixture containing 40% wt. DMAE and 5% wt. MAPA over a temperature range from 313.15 to 358.15 K. Among the different mixtures evaluated, DMAE + MAPA emerged as the most promising in terms of CO_2 absorption capacity.

Therefore, to expand the thermodynamic knowledge of new promising amine blends, one of the objectives of this work was to study the Vapour-Liquid Equilibrium (VLE) of CO_2 in aqueous DMAE (30% wt.) + MAPA (10% wt.) at different temperatures (313.15, 333.15 and 363.15) K. The selected concentrations were chosen to provide a balance between reactivity [18,19], solvent stability, and acceptable transport properties, since higher amine fractions can significantly increase viscosity and affect cyclic capacity, as shown in previous studies [13–15]. Additionally, we investigated the physical solubility of CO_2 in this system using the N_2O/CO_2 analogy. The techniques employed in this work for VLE measurements are predominantly based on synthetic-static methods. Also, density measurements of the aqueous amine mixture were carried out since they are needed in those calculations. Finally, we have developed empirical and semi-empirical models to correlate experimental data as a function of temperature and pressure.

2. Materials and experimental procedures

2.1. Materials

Analytical grade MEA, DMAE and MAPA were purchased from Sigma-Aldrich. Research grade CO_2 and N_2O were used, and their features are detailed in Table 1. High-purity water was employed for solution preparation. Specifically, in-house produced high-purity water was used for the preparation of solutions used in physical N_2O solubility measurements conducted at the Thermophysical Laboratory, Imperial College London. An analytical balance Mettler Toledo (PR/SR series) was available to prepare the solutions. For VLE measurements of CO_2 performed at the Termocal Laboratory, University of Valladolid, commercially sourced high-purity water was used. In this case, aqueous amine solutions were prepared using an analytical balance (Radwag scale model PS750/C/2) with a resolution of 1 mg. The standard uncertainty of amine mass fraction is 0.0001 for both balances. For storage, the solutions were kept in sealed containers in a dark environment, to minimize degradation from atmospheric oxygen and reaction with ambient carbon dioxide. The maximum storage time prior to use was two days.

Table 1
Description of chemical samples and gases. Here x denotes the mole fraction, ρ_e denotes electrical resistivity at $T = 298$ K and w denotes the mass fraction.

Compound	CAS number	Source	Purity[a]	Water content (%)[b]	Additional purification
Physical solubility of N_2O (Imperial College London)					
N_2O	10024-97-2	BOC	$x \geq 0.99997$		None
H_2O	7732-18-5	Produced in house by reverse osmosis	$\rho_e \geq 18.2$ MΩ·cm		Degassed[f]
DMAE[c]	108-01-0	Sigma-Aldrich	$w \geq 0.999$	0.04	Degassed[f]
MAPA[d]	6291-84-5		$w \geq 0.991$	0.26	Degassed[f]
CO_2 solubility and density measurements (University of Valladolid)					
CO_2	124-38-9	Air Liquide	$x \geq 0.999995$		None
H_2O	7732-18-5	Honeywell	Conductivity $\leq 2{\cdot}10^{-6}$ $\Omega^{-1}{\cdot}cm^{-1}$		Degassed[g]
MEA[e]	141-43-5	Sigma-Aldrich	$w \geq 0.997$	0.15	Degassed[h]
DMAE[c]	108-01-0		$w \geq 0.998$	0.18	Degassed[h]
MAPA[d]	6291-84-5		$w \geq 0.991$	0.26	Degassed[h]

[a] As stated by the supplier.
[b] Karl Fischer method.
[c] DMAE = 2-Dimethylaminoethanol.
[d] MAPA = N-Methyl-1,3-propanediamine.
[e] MEA = Monoethanolamine.
[f] Under vacuum at room temperature.
[g] Vacuum distillation with ultrasonic bath.
[h] Freeze-pump-thaw method.

2.2. Density of aqueous amine blend

Accurate volumetric data are essential for calculating the solvent mass introduced into the reactor when using the synthetic-static method to determine the physical solubility of N_2O in aqueous amines. Consequently, density of the aqueous amine solutions was measured using a vibrating tube densimeter (DMA 512P) with a technique like that shown by Segovia et al. [20].

The technique covers a density range of (0–3000) kg·m^{-3}, with a resolution of 10^{-2} kg·m^{-3}. Its operation is automated using a custom-developed code implemented in LabVIEW software. Measurement of oscillation periods is conducted using a frequency counter (Keysight 53220 A). Temperature within the densimeter is measured using a calibrated Pt100 probe with an expanded uncertainty of 0.02 K and a pressure indicator Druck DPI 145 gives pressure with an expanded uncertainty of 0.02 MPa.

Density uncertainty assessment was performed using the Guide to the Expression of Uncertainty in Measurement [21] and resulted in an expanded uncertainty $U(\rho) = 0.7$ kg/m^3, with a coverage factor $k = 2$, providing a confidence level of approximately 95.5%. The uncertainty budget includes contributions from repeatability, temperature and pressure measurements, and densimeter calibration which is the main contribution. The potential contribution derived from chemical purity, considering the low levels of impurities in the compounds used, is estimated negligible compared to other contributions. The details of these calculations are reported in [20].

The densimeter was calibrated using water and vacuum over the whole working temperature and pressure ranges, at temperature from (273.15 to 393.15) K and pressure up to 70 MPa. The density of water was calculated using the IAPWS-95 formulation for water [22], as implemented in REFPROP NIST v10.0 database [23]. The relative uncertainties of the reference density values in liquid phase are 0.0001% at atmospheric pressure; 0.001% for pressures up to 10 MPa and 0.003% up to 100 MPa and temperatures up to 423 K. The vibrating period, τ, is related to the density of the fluid following the equation proposed by Lagourette et al. [24] and modified by Comuñas et al. [25]:

$$\rho(T,p) = A(T)\tau^2(T,p) - B(T,p) \tag{1}$$

where $A(T)$ and $B(T,p)$ are two parameters which are obtained from the calibration of the apparatus at each temperature and pressure measured:

$$A(T) = \frac{\rho_{\mathrm{ref}}(T, 0.1\ \mathrm{MPa})}{\tau^2_{\mathrm{ref}}(T, 0.1\ \mathrm{MPa}) - \tau^2_{\mathrm{vacuum}}(T)} \tag{2}$$

$$B(T,p) = \frac{\rho_{\mathrm{ref}}(T, 0.1\ \mathrm{MPa})}{\tau^2_{\mathrm{ref}}(T, 0.1\ \mathrm{MPa}) - \tau^2_{\mathrm{vacuum}}(T)}\tau^2_{\mathrm{ref}}(T,p) - \rho_{\mathrm{ref}}(T,p) \tag{3}$$

where the subscript "ref" is referred to water or other fluid with well-characterized density.

2.3. Measuring N_2O solubilities in aqueous amines mixtures

The experiments were conducted using a synthetic-static method, as originally described by Torín-Ollarves and Trusler [26]. For a detailed description of the experimental setup and procedure please refer to the work of Chen and Trusler [27]. A brief overview of the equipment is provided as follows.

The equilibrium cell is a titanium grade 5 monobloc vessel with an approximate internal volume of 90 cm^3. It is closed with a sapphire window (50 mm diameter × 25 mm thickness) sealed by an EPDM O-ring with a phosphor-bronze anti-extrusion ring. The system can operate at pressures up to 70 MPa and temperatures up to 473.15 K. To ensure uniform heating, the cell is surrounded by an aluminium jacket equipped with four electric cartridge heaters. The temperature is monitored using a platinum resistance thermometer (PRT) probe with a standard uncertainty of $u(T) = 0.03$ K. The external surface of the jacket is insulated with a thick layer of silicone-rubber sponge. A glass-encased stirrer bar (6 mm diameter × 25 mm long) with a FEP sleeve is used for agitation. The bar is driven by a pair of magnets rotated by a variable-speed motor at up to 1400 rpm. A stirring velocity of approximately 350 rpm was maintained to ensure adequate mixing within the cell. To observe the phase behaviour, a CCD camera with a zoom lens was positioned to view through the sapphire window. Two pressure sensors were employed: one to measure the initial gas injection pressure (Keller model PAA-35X, $p < 3$ MPa) and the other to measure the equilibrium pressure within the cell during solvent injection (Keller model PA-35X, $p < 70$ MPa). Both pressure sensors have a relative standard uncertainty of $u_r(p) = 0.03\%$ of their respective full-scale readings. Prior to experiments, the aqueous amine solution was placed in a glass bottle and degassed under vacuum with stirring using a vacuum pump (Vacuubrand model MZ 2C NT) until a pressure lower than $5{\cdot}10^{-2}$ hPa was achieved. The solution was then drawn into a previously evacuated high pressure syringe pump (Teledyne ISCO model 100 DM) from which it was subsequently injected into the equilibrium cell. Pressure, volume, temperature, and volumetric flow were recorded at each equilibrium point. A chiller with recirculating water was used to maintain the syringe pump at a temperature of at approximately 291.15 K.

2.4. Determination of bubble pressure

Bubble pressure estimation can be achieved through a graphical approach and empirical fittings as described by Torín-Ollarves and Trusler [26]. The graphical method involves plotting liquid-gas equilibrium pressures against the injected solvent quantity. Subsequently, curves are fitted to the data within each region: a linear function for the single-liquid phase and, typically, a polynomial curve for the two-phase region. The point of intersection between these curves is the bubble pressure. However, this graphical method shows variability due to the fitting process and the choice of polynomial functions. In certain systems, such as CO + brines, fitting the reciprocal of the equilibrium pressure has been found to enhance the accuracy of the two-phase region fit [27]. In such cases, single-liquid phase region is represented by the reciprocal of a linear function of the amount of the injected solvent, while two-phase region is almost described by a linear trend. For the Amine + H_2O + N_2O system, the high solubility leads to a pronounced change in slope between the phases, thereby simplifying the determination of bubble pressure without the need for the inverse graphical approximation proposed by Kling and Maurer [28].

The internal extrapolation uncertainty of the bubble pressure, $u_{\mathrm{int}}(p_b)$, obtained from the standard uncertainty of the fitted intersection derived from the variance-covariance matrix of the regression, ranged between (0.03–0.24) MPa, with most values below 0.09 MPa.

The relative standard uncertainty of the bubble-point pressure was calculated as:

$$u_r^2(p_b) = u_r^2(p) + u_{\mathrm{int}}^2(p_b)/p_b^2 \tag{4}$$

where p_b denotes the bubble pressure, detailed information is provided in [27].

2.5. Measuring CO_2 solubilities in aqueous amines mixtures

CO_2 solubility in aqueous amines was measured using a synthetic-static apparatus, originally proposed by Gibbs and Van Ness [29] which is shown in Fig. 1. The core of the equipment is a stainless steel (AISI-316 L) equilibrium cell capable of operating at pressures up to 10 MPa and temperatures up to 393.15 K. Pressure was measured in two ranges: a DPI 104 pressure sensor with an expanded uncertainty of 0.05% ($k = 2$) for $p < 0.2$ MPa, and an Additel model 686 digital pressure gauge with an expanded uncertainty of 0.02% ($k = 2$) of full scale for $0.2 < p < 14$ MPa. The cell was immersed in a thermostatic bath

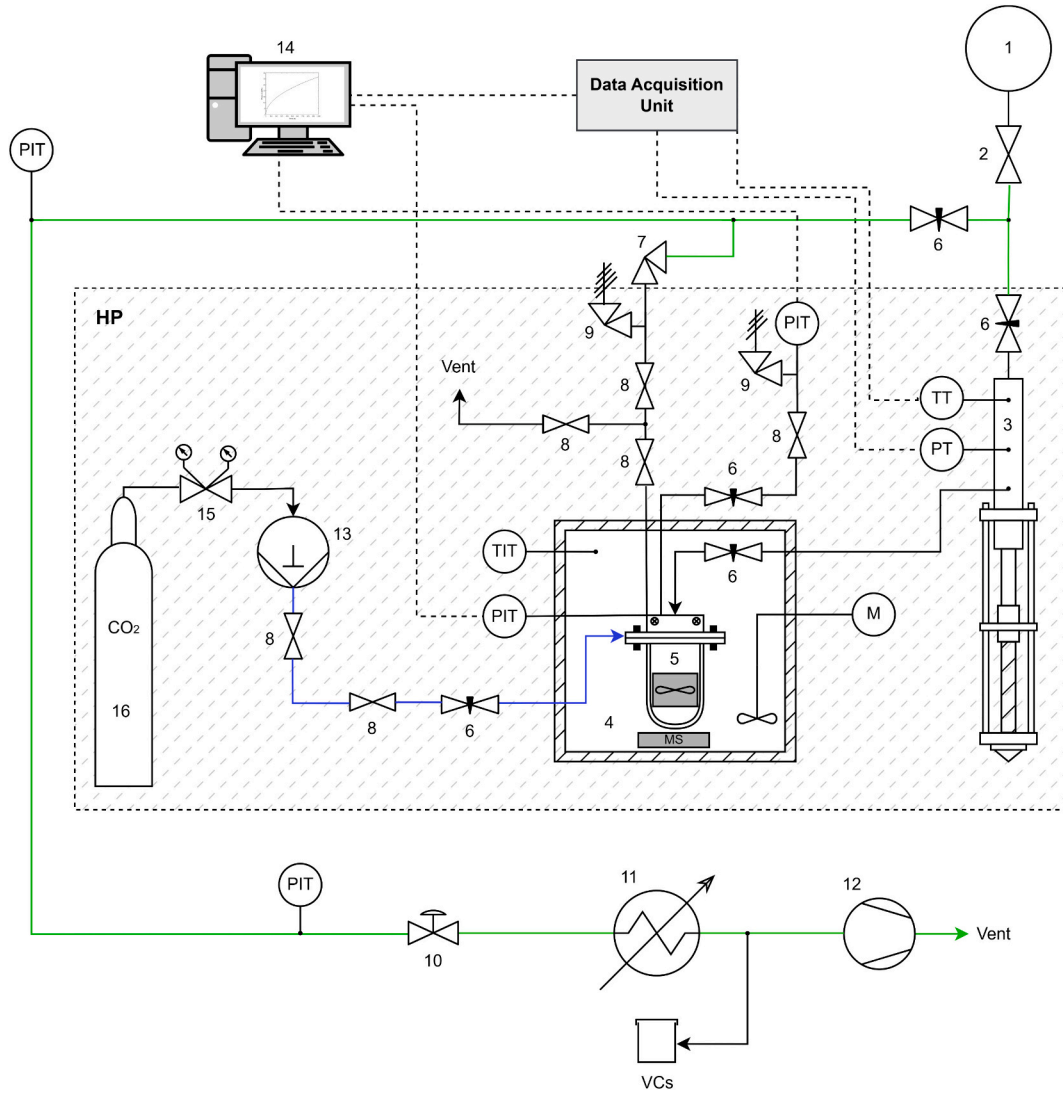

Fig. 1. Schematic diagram of the synthetic-static apparatus for VLE measurements. 1: Bottle with degassed water; 2: Plug valve; 3: Liquid-metering pump; 4: Thermostatic bath; 5: Equilibrium cell; 6: Needle valve; 7: Right angle valve; 8: Ball valve; 9: Relief valve; 10: Speedivalve; 11: Dewar flask; 12: Vacuum pump; 13: ISCO pump; 14: Computer; 15: Pressure regulator; 16: Gas cylinder; PIT: Transmitter and indicator of pressure; PT: Transmitter of pressure; TIT: Transmitter and indicator of temperature; TT: Transmitter of temperature; HP: High pressure zone; MS: Magnetic stirrer; VCs: Volatile compounds; M: Induction motor; Green line: Vacuum line; Blue line: Isolated capillary tube. (For interpretation of the references to colour in this figure legend, the reader is referred to the web version of this article.)

(Hart Scientific 6020) filled with silicon oil, providing a stable temperature of ±0.01 K. Inside the cell, a magnetic stirrer ensured thorough mixing of the aqueous amine solution. To prepare the solution, a known amount of pure amine was weighed using a precision balance (Radwag scale model PS750/C/2) with a resolution of 1 mg. The pure amine was then degassed using the freeze-pump-thaw cycling method until reaching vacuum pressures of 0.1 Pa. Degassed water was introduced into the cell using a liquid metering pump (Ruska model 2200–801) with an expanded uncertainty of 0.03 ml ($k = 2$). This piston was equipped with a Druck PTX 1400 pressure transmitter (0–4 MPa) and a Pt100 thermoresistance connected to an Agilent 34970 A data acquisition unit. By correlating pressure and temperature measurements with displaced volume data from the REFPROP NIST v10.0 database, the required mass for a specific mass composition of aqueous amine was calculated [22,23]. The density of the water used for solvent preparation had a relative standard uncertainty of 0.001%. The volume of the cell was accurately determined, depending on temperature, by calibration with water as: $V^T/\text{ml} = 179.04–0.0353{\cdot}T(\text{K}) + 5.87{\cdot}10^{-5}{\cdot}T^2(\text{K})$ for $p < 160$ kPa and $V^T/\text{ml} = 178.38–0.0353{\cdot}T(\text{K}) + 5.87{\cdot}10^{-5}{\cdot}T^2(\text{K})$ for $p > 160$ kPa with an uncertainty of 0.36 ml.

An ISCO pump (model 260D) was used to introduce the necessary mass of CO_2 loading, with an estimated relative standard uncertainty of mass injected of $u_r(m^T_{CO_2}) = 0.2\%$. The density of CO_2 (ρ_{CO_2}) is estimated with the EoS presented by Span and Wagner [30] and integrated into the REFPROP NIST v10.0 database [23] (relative standard uncertainty of $u_r(\rho_{CO_2}) = 5{\cdot}10^{-4}$). A new gas charge is initiated when equilibrium pressure of cell is achieved taking a time between six and eight hours.

Following the methology applied by other authors [18,19], the partial pressure of CO_2 was calculated from the experimental results for the total pressure by sustracting the vapour pressure of aqueous amine mixture and the solubility of CO_2 can be estimated through a mass balance:

$$m^L_{CO_2} = m^T_{CO_2} - m^V_{CO_2} = m^T_{CO_2} - \rho_{CO_2} V^V = m^T_{CO_2} - \rho_{CO_2}\left(V^T - V^L\right) = m^T_{CO_2} - \rho_{CO_2}\left(V^T - \frac{m^L}{\rho^L}\right) \quad (5)$$

where $m^T_{CO_2}$, $m^L_{CO_2}$ and $m^V_{CO_2}$ are the mass of CO_2 injected to the cell, mass

of CO_2 solubilized in the liquid phase and mass of CO_2 in the vapour phase, respectively. V^T, V^L and V^V represent the total volume of the cell, volume of the liquid phase, and volume of the vapour phase, respectively. Also, ρ_{CO_2} and ρ^L denote the density of pure CO_2 (at the partial pressure of the CO_2 and cell temperature) and the density of the liquid phase, respectively.

The CO_2 loading in aqueous amine (α_{exp}) is defined by Eq. (6). The uncertainty of this value is determined from the combined uncertainties of the mass of CO_2 in the liquid phase ($m^L_{CO_2}$) and the total mass of amine (m^L_{am}) as shown in Table 2 and Eq. (7). The uncertainty associated with the mass of amine $u(m^L_{am})$ used was estimated based on the calibration accuracy of the balance and the purity of the amine reagent. Similarly, the uncertainty in the mass of CO_2 in the liquid phase $u\left(m^L_{CO_2}\right)$ was determined taking into account the following contributing factors: uncertainty of the mass of CO_2 injected from the ISCO pump $u\left(m^T_{CO_2}\right)$ and uncertainty in the mass of CO_2 in the vapour phase $u\left(m^V_{CO_2}\right)$. The uncertainty associated with the molar masses of pure components is considered negligible.

$$\alpha_{exp}\left[\frac{\text{mol}-CO_2}{\text{mol}-\text{amine}}\right]=\frac{n_{CO_2}}{n_{am}}=\frac{m^L_{CO_2}}{m^L_{am}}\cdot\left(\frac{M_{am}}{M_{CO_2}}\right) \tag{6}$$

$$u_c(\alpha_{exp})=\left[\left(\frac{\partial f}{\partial m^L_{CO_2}}\right)^2 u^2\left(m^L_{CO_2}\right)+\left(\frac{\partial f}{\partial m^L_{am}}\right)^2 u^2\left(m^L_{am}\right)\right]^{0.5} \tag{7}$$

where M_{am}, M_{CO_2}, n_{CO_2}, and n_{am} represent the average molar mass of the amine, the molar mass of CO_2, and the total moles of CO_2 and amine in the liquid phase, respectively.

The setup was validated by solubility measurements of CO_2 in a 30% wt. aqueous solution of MEA at 313.15 K (Fig. 2). Experimental data are reported in Table 3. The validation demonstrates reliable performance even at low CO_2 partial pressures where the measurement uncertainty increases. For instance, at $p_{CO_2} \sim 1$ kPa, the relative expanded uncertainty is $U_r(p_{CO_2}) = 13\%$ ($k = 2$).

3. Modelling framework

3.1. Physical solubility

A suitable model to describe the solubility of N_2O in aqueous amine solutions, $H_{N_2O,solution}$, across a wide temperature and pressure range is the Krichevsky-Ilinskaya (KI) equation:

Table 2
Contributions to uncertainty for the measurement of CO_2 solubility in an aqueous mixture with DMAE (30% wt.) and MAPA (10% wt.)

Source of uncertainty	Uncertainty	Unit	Value
CO_2 loading	$u(\alpha_{exp})/\alpha_{exp}$	–	0.003–0.048
Addition of CO_2	$u\left(m^T_{CO_2}\right)/m^T_{CO_2}$	–	0.002
Pump temperature	$u(T_{pump})$	K	0.1
Pump pressure	$u(p_{pump})$	MPa	0.013
Density of CO_2 added	$u(\rho_{add})$	kg·m^{-3}	0.48
Volume added	$u(V_{add})/V_{add}$	–	0.002
CO_2 mass in vapour phase	$u\left(m^V_{CO_2}\right)/m^V_{CO_2}$	–	0.05–0.14
Calibration of the cell volume	$u(V^T)$	ml	0.36
Liquid volume	$u(V^L)$	ml	2–6
Density of the gas phase (CO_2)	$u(\rho_{CO_2})/\rho_{CO_2}$	–	$5\cdot10^{-4}$ - 0.04
CO_2 mass in liquid phase	$u\left(m^L_{CO_2}\right)/m^L_{CO_2}$	–	0.002–0.05
Amine mass in liquid phase	$u\left(m^L_{am}\right)/m^L_{am}$	–	0.003

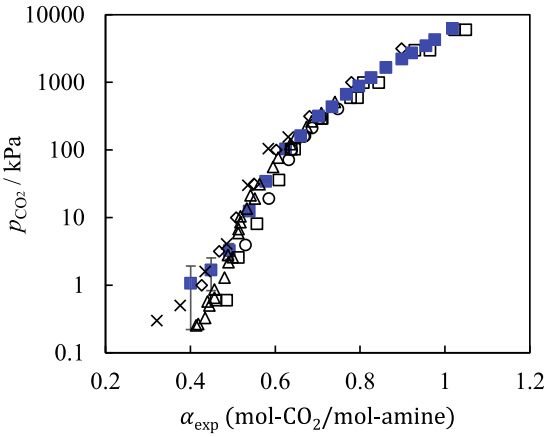

Fig. 2. Comparison of solubility data of CO_2 in 30% wt. aqueous MEA at T = 313.15 K: (■) this work; (□) Jou et al. [31]; (○) Tong et al. [32]; (△) Bernhardsen et al. [8]; (✖) Feng et al. [33]; (◇) Lee et al. [34].

Table 3
Total pressure, p, CO_2 partial pressure, p_{CO_2}, and experimental CO_2 loading α_{exp} (mol-CO_2/mol-amine), in aqueous ~30% wt. MEA solution at T = 313.15 K[d].

p/kPa[a]	p_{CO_2}/kPa	α_{exp}	$U(\alpha_{exp})$[b]	$U_r(\alpha_{exp})$
w_{MEA} = 0.2983[c]				
6.62		0		
8.30	1.68	0.449	0.002	0.4%
19.18	12.56	0.539	0.002	0.4%
110.68	104.06	0.625	0.002	0.4%
324.7	318.1	0.702	0.003	0.4%
678.0	671.4	0.768	0.003	0.4%
1186.5	1179.9	0.826	0.004	0.5%
2238.2	2231.5	0.898	0.006	0.7%
3508.2	3501.6	0.955	0.010	1.0%
w_{MEA} = 0.2988[c]				
6.31		0		
7.38	1.07	0.401	0.001	0.4%
9.57	3.26	0.492	0.002	0.4%
40.71	34.40	0.578	0.002	0.4%
169.3	163.0	0.660	0.002	0.4%
442.7	436.4	0.734	0.003	0.4%
888.5	882.2	0.797	0.003	0.4%
1665.9	1659.6	0.861	0.005	0.5%
2750.7	2744.4	0.922	0.007	0.8%
4297.3	4291.0	0.976	0.013	1.3%
6302.9	6296.6	1.018	0.023	2.3%

[a] Expanded uncertainty in pressure $U(p) = 0.11$ kPa for $p < 160$ kPa and $U(p) = 2.8$ kPa for $p > 160$ kPa reported with a coverage factor of $k = 2$.
[b] Expanded uncertainty in CO_2 loading $U(\alpha)$ reported with a coverage factor of $k = 2$.
[c] Standard uncertainty of amine mass fraction $u(w_i) = 0.0001$.
[d] Standard uncertainty of temperature $u(T) = 0.02$ K.

$$\ln\left(\widehat{f}_{N_2O}/b_{N_2O}\right)=\ln H_{N_2O}+\frac{\overline{v}^{\infty}_{N_2O}\left(p-p^{sat}_s\right)}{RT}+\frac{A}{RT}\left(x_s^2-1\right) \tag{8}$$

where $\widehat{f}_{N_2O}$ is the fugacity of N_2O in the gas phase, b_{N_2O} is the molality of N_2O in the liquid phase (mol/kg-solution), x_s is the mole fraction of the solvent and p^{sat}_s is the saturation pressure of solvent. In this analysis, the liquid-phase fugacity of the solute is a simple function of the Henry's constant $H_{N_2O,solution}$, the partial molar volume of N_2O at infinite dilution $\overline{v}^{\infty}_{N_2O}$ is assumed to be independent of the pressure and the activity coefficient of the solute is normalized by a two-suffix Margules parameter A [35]. A linear trend is yielded by plotting $\ln\left(\widehat{f}_{N_2O}/b_{N_2O}\right)-\overline{v}^{\infty}_{N_2O}\left(p-p^{sat}_s\right)/RT$ against $\left(x_s^2-1\right)$; A/RT is the slope, while the intercept is $\ln H_{N_2O}$.

The mole fraction of aqueous amine in the gas phase (y_s) is

determined by Raoult's law:

$$y_s = p_s^{sat}/p \tag{9}$$

The fugacity of N_2O in the gas phase is given by:

$$\widehat{f}_{N_2O} = (1 - y_s)\phi^*_{N_2O} p \tag{10}$$

where $\phi^*_{N_2O}$ denotes the fugacity coefficient of N_2O, taken as that of the pure gas and calculated with the REFPROP NIST v10.0 database [23].

To the best of our knowledge, volumetric data and correlations for the molar volume of N_2O at infinite dilution in mixtures with DMAE and MAPA are currently unavailable. As suggested by Jou et al. [36] and Monteiro and Svendsen [37], it is reasonable to approximate the molar volume of N_2O with that of CO_2 in water, given their similar molecular structures and comparable behaviour in solvent systems. For this reason, the correlation of Brelvi and O'Connell to calculate $\bar{v}^{\infty}_{N_2O}$ [38] is used.

3.2. Chemical equilibria

Aqueous amine mixtures with DMAE, MAPA and CO_2 undergo a set of chemicals reactions involving ionic species (Eqs. (11)–(17)). According to Zoghi et al. [19], the reaction mechanism is described as follows:

a) Dissociation of protonated DMAE:

$$DMAEH^+_{(aq)} + H_2O_{(l)} \Leftrightarrow^{K_1} DMAE_{(aq)} + H_3O^+ \tag{11}$$

b) Dissociation of protonated MAPA:

$$MAPAH^+_{(aq)} + H_2O_{(l)} \Leftrightarrow^{K_2} MAPA_{(aq)} + H_3O^+ \tag{12}$$

c) Dissociation of diprotonated MAPA:

$$+HMAPAH^+_{(aq)} + H_2O_{(l)} \Leftrightarrow^{K_3} MAPAH^+_{(aq)} + H_3O^+ \tag{13}$$

d) Formation of carbamate:

$$MAPA_{(aq)} + CO_{2(l)} + H_2O_{(l)} \Leftrightarrow^{K_4} MAPACOO^-{}_{(aq)} + H_3O^+ \tag{14}$$

e) Dissociation of bicarbonate ion:

$$HCO_3^-(aq) + H_2O_{(l)} \Leftrightarrow^{K_5} CO_3^{2-}(aq) + H_3O^+ \tag{15}$$

f) Dissociation of CO_2:

$$CO_{2(aq)} + 2H_2O_{(l)} \Leftrightarrow^{K_6} HCO_3^-(aq) + H_3O^+ \tag{16}$$

g) Dissociation of water:

$$2H_2O_{(l)} \Leftrightarrow^{K_7} H_3O^+ + OH^-_{(aq)} \tag{17}$$

The reactions described by Eq. (15), Eq. (16) and Eq. (17) are the dissociation of bicarbonate ions, CO_2 and water, respectively. Dissociation of protonated amine (DMAE and MAPA) and formation of carbamate are described in Eq. (11) to Eq. (14). Equilibrium constants and temperature-dependent coefficients were correlated using the initial Zoghi et al. [19] parameters. The reaction mechanism represented by this set of equations is analogous to those reported in the literature for binary amine blends, specifically those incorporating a diamine [39]. These species in the liquid phase are: DMAE, $DMAEH^+$, MAPA, $MAPA^+$, + $HMAPAH^+$, $MAPACOO^-$, H_2O, H_3O^+, OH^-, CO_2, CO_3^{2-}, HCO_3^-.

The equilibrium constants for the given equations are:

$$K_1 = \frac{(\gamma_{DMAE} b_{DMAE})(\gamma_{H_3O^+} b_{H_3O^+})}{(\gamma_{DMAEH^+} b_{DMAEH^+})(\gamma_{H_2O} b_{H_2O})} \tag{18}$$

$$K_2 = \frac{(\gamma_{MAPA} b_{MAPA})(\gamma_{H_3O^+} b_{H_3O^+})}{(\gamma_{MAPAH^+} b_{MAPAH^+})(\gamma_{H_2O} b_{H_2O})} \tag{19}$$

$$K_3 = \frac{(\gamma_{MAPAH^+} b_{MAPAH^+})(\gamma_{H_3O^+} b_{H_3O^+})}{(\gamma_{+HMAPAH^+} b_{+HMAPAH^+})(\gamma_{H_2O} b_{H_2O})} \tag{20}$$

$$K_4 = \frac{(\gamma_{MAPACOO^-} b_{MAPACOO^-})(\gamma_{H_3O^+} b_{H_3O^+})}{(\gamma_{MAPA} b_{MAPA})(\gamma_{CO_2} b_{CO_2})(\gamma_{H_2O} b_{H_2O})} \tag{21}$$

$$K_5 = \frac{\left(\gamma_{CO_3^{2-}} b_{CO_3^{2-}}\right)(\gamma_{H_3O^+} b_{H_3O^+})}{\left(\gamma_{HCO_3^-} b_{HCO_3^-}\right)(\gamma_{H_2O} b_{H_2O})} \tag{22}$$

$$K_6 = \frac{\left(\gamma_{HCO_3^-} b_{HCO_3^-}\right)(\gamma_{H_3O^+} b_{H_3O^+})}{(\gamma_{CO_2} b_{CO_2})(\gamma_{H_2O} b_{H_2O})^2} \tag{23}$$

$$K_7 = \frac{(\gamma_{OH^-} b_{OH^-})(\gamma_{H_3O^+} b_{H_3O^+})}{(\gamma_{H_2O} b_{H_2O})^2} \tag{24}$$

where b_i and γ_i are molality and activity coefficient for species i in the solution, respectively. In addition to the equilibrium equations, the mass balances for the whole set of species involved in chemical reaction are described as follows:

Mass balance for DMAE and MAPA in the liquid phase:

$$b_{DMAE,t} = b_{DMAE} + b_{DMAEH^+} \tag{25}$$

$$b_{MAPA,t} = b_{MAPA} + b_{MAPAH^+} + b_{+HMAPAH^+} + b_{MAPACOO^-} \tag{26}$$

Mass balance for CO_2 in the liquid phase:

$$b_{CO_{2,t}} = \alpha_{CO_2} b_{t,am} = b_{CO_2} + b_{HCO_3^-} + b_{CO_3^{2-}} + b_{MAPACOO^-} \tag{27}$$

And the electroneutrality condition for the solution:

$$b_{H_3O^+} + b_{DMAEH^+} + b_{MAPAH^+} + 2b_{+HMAPAH^+} = b_{OH^-} + b_{HCO_3^-} + 2b_{CO_3^{2-}} + b_{MAPACOO^-} \tag{28}$$

where α_{CO_2} is the CO_2 loading (mol-CO_2/mol-amine) and $b_{t,am}$ the total amine concentration in a molality scale. In the thermodynamic modelling framework with CO_2, concentrations (b_i) are expressed on a molality basis with respect to water (mol/kg-H_2O).

3.3. Thermodynamic modelling

Activity coefficients (γ_i) for all species in the liquid phase were calculated using the Deshmukh-Mather (D-M) model [40–44]. It is important to note that the D-M model provides a flexible framework that requires system-specific interaction parameters $\left(\beta_{ij}\right)$. Furthermore, the equilibrium between gas and liquid phase is described with a gamma-phi ($\gamma - \phi$) equation:

$$y_w \phi_w p = a_w \phi^s_w p^{sat}_w \exp\left(\frac{v_w (p - p^{sat}_w)}{RT}\right) \tag{29}$$

$$y_{CO_2} \phi_{CO_2} p = \gamma_{CO_2} b_{CO_2} H_{CO_2} \exp\left(\frac{\bar{v}^{\infty}_{CO_2} (p - p^{sat}_w)}{RT}\right) \tag{30}$$

where ϕ_i, p_i, v_i are, respectively, fugacity coefficient, partial pressure, and molar volume of component i (water and CO_2). R is the gas constant. Vapour pressure p^{sat}_w and partial molar volume v_w of water are calculated based on equations form Saul and Wagner [45]. The correlation of Brelvi

and O'Connell is used to calculate the partial molar volume $\bar{v}^{\infty}_{CO_2}$ of CO_2 in water at infinite dilution [38]. The binary interaction parameters between ion-ion, ion-molecule, and molecule-molecule $\left(\beta_{ij}\right)$ included in $\gamma-\phi$ model are optimized as a function of temperature:

$$\beta_{ij} = A_{ij}T^3 + B_{ij}T^2 + C_{ij}T + D_{ij} \tag{31}$$

where A_{ij}, B_{ij}, C_{ij} and D_{ij} are regressed parameters depending on experimental data as shown in Table 4. The model equations for equilibrium constants, mass balances, and the D-M model were implemented and solved in MATLAB.

3.4. Optimization procedure

The Levenberg-Marquardt method is used in order to minimize the objective function of least squares (Eq. 32) and the models were assessed with the Average Absolute Deviation (AAD), maximum average deviation (MAD) and the standard deviation of the adjustment (σ) defined by Eqs. (33)–(35).

$$\mathrm{OF} = \frac{1}{n}\sum_{i=1}^{n}\left(X_{c,i} - X_{exp,i}\right)^2 \tag{32}$$

$$\mathrm{AAD}, X = \frac{1}{n}\sum_{i=1}^{n}\frac{\left|X_{c,i} - X_{exp,i}\right|}{X_{exp,i}} \tag{33}$$

$$\mathrm{MAD}, X = \max\left(\frac{\left|X_{c,i} - X_{exp,i}\right|}{X_{exp,i}}\right) \tag{34}$$

$$\sigma = \sqrt{\left[\frac{1}{n-P}\right]\sum_{i=1}^{n}\left(X_{c,i} - X_{exp,i}\right)^2} \tag{35}$$

where n is the total number of data points, P is the number of fitting parameters. $X_{c,i}$ is the ith model-predicted value of a defined property X and $X_{exp,i}$ is the ith experimentally measured value. The evaluated properties comprise the liquid solvent density (ρ), determined by fitting experimental data to a modified Tammann-Tait equation; the Henry's constant of CO_2 (H_{CO_2}), obtained from a second-order polynomial expression; the CO_2 partial pressure (p_{CO_2}), estimated using an empirical soft model; and the CO_2 loading (α_{CO_2}), calculated through the thermodynamic $(\gamma-\phi)$ (model).

4. Results and discussion

4.1. Density measurement

Density measurements of the aqueous mixture containing DMAE (30% wt.) and MAPA (10% wt.) were performed at pressures from (0.1 to 70) MPa and at seven temperatures from (293.15 to 393.15) K. At temperatures of 373.15 K and 393.15 K, a minimum pressure of 1 MPa was applied to prevent bubble formation in the vibrating tube densimeter. The experimental results are presented in Table 5.

The densities of the aqueous amine mixture have been correlated using a modified Tammann-Tait (TT) equation:

$$\rho = \frac{\rho\left(T, p_{ref}\right)}{1 - C\ln\left(\frac{B(T)+p}{B(T)+p_{ref}}\right)} \tag{36}$$

Table 5
Experimental densities, ρ, of the aqueous mixture with DMAE ($w_{DMAE} = 0.2995$) and MAPA ($w_{MAPA} = 0.0997$) at different conditions of temperature, T, and pressure, p.[a]

p/MPa	ρ/(kg·m^{-3})						
	T/K						
	293.15	313.15	333.15	353.15	363.15	373.15	393.15
0.1	985.4	971.2	955.8	939.3	930.7		
0.5	985.6	971.4	955.9	939.5	930.8		
1	985.8	971.6	956.1	939.7	931.1	922.1	903.1
2	986.2	972.0	956.6	940.2	931.6	922.7	903.7
3	986.6	972.4	957.0	940.7	932.1	923.2	904.3
5	987.3	973.2	957.9	941.7	933.1	924.3	905.5
6	987.7	973.6	958.3	942.1	933.6	924.8	906.1
9	988.8	974.7	959.6	943.6	935.1	926.3	907.9
10	989.1	975.1	960.0	944.0	935.6	926.9	908.4
12	989.9	975.9	960.9	945.0	936.6	927.9	909.6
15	990.9	977.1	962.2	946.3	938.0	929.4	911.3
20	992.7	979.0	964.2	948.6	940.4	931.9	914.0
25	994.5	980.8	966.3	950.8	942.7	934.4	916.8
30	996.2	982.6	968.3	953.0	945.0	936.8	919.4
35	997.9	984.6	970.2	955.2	947.3	939.1	921.9
40	999.6	986.4	972.3	957.3	949.4	941.4	924.4
50	1002.9	989.9	976.0	961.4	953.8	945.9	929.3
60	1006.2	993.4	979.7	965.4	957.9	950.2	934.0
70	1009.4	996.8	983.3	969.3	961.9	954.3	938.6

[a] Expanded uncertainties ($k = 2$): $U(T) = 0.02$ K; $U(p) = 0.02$ MPa; $U(w) = 0.0002$ and $U(\rho) = 0.7$ kg·m^{-3}.

Table 4
Optimized interaction parameters of Deshmukh-Mather (D-M) model.

β_{ij}	$A_{ij}\cdot10^{-10}$/(kg·mol^{-1}·K^{-3})	$B_{ij}\cdot10^{-6}$/(kg·mol^{-1}·K^{-2})	$C_{ij}\cdot10^{-4}$/(kg·mol^{-1}·K^{-1})	$D_{ij}\cdot10^{-2}$/(kg·mol^{-1})
$\beta_{DMAEH^+-MAPACOO^-}$	−70.20	−0.53	1.76	−2.81
$\beta_{DMAEH^+-CO_2}$	10.37	−2.51	2.84	−16.97
β_{DMAEH^+-DMAE}	11.70	−5.08	28.61	−26.10
$\beta_{MAPAH^+-MAPACOO^-}$	−42.40	−4.32	−11.37	2.53
$\beta_{MAPAH^+-CO_2}$	0.23	0.78	−4.10	1.18
$\beta_{MAPAH^+-HCO_3^-}$	5.36	−2.19	−0.01	−16.77
β_{MAPAH^+-DMAE}	125.22	−6.76	4.59	−33
β_{MAPAH^+-MAPA}	12.22	0.67	−15.29	9.99
$\beta_{MAPACOO^--CO_2}$	0.14	14.09	0.06	2.88
$\beta_{MAPACOO^--DMAE}$	0.13	0.99	46.77	−243.47
$\beta_{MAPACOO^--MAPA}$	−17.04	2.51	22.75	6.73
$\beta_{CO_2-HCO_3^-}$	0.05	1.26	−5.97	4.98
β_{CO_2-DMAE}	−3.32	0.63	−2.78	3.15
β_{CO_2-MAPA}	−21.58	0.76	−1.88	9.14
$\beta_{HCO_3^--DMAE}$	−20.77	6.03	−0.90	19.77
$\beta_{HCO_3^--MAPA}$	−148.50	4.53	−16.96	33.89
$\beta_{DMAE-MAPA}$	37.63	−1.47	8.12	−2.90

Table 6
Fitting parameters of Eqs. (36)–(38) and their standard uncertainties for the density measurements. Standard deviations σ, absolute average deviation (AAD) and maximum average deviation (MAD) for Tammann-Tait correlation.

Parameter	Value	Standard uncertainty
A_0/(kg·m^{-3})	1059	4
A_1/(kg·m^{-3}·K^{-1})	0.2	0.02
A_2/(kg·m^{-3}·K^{-2})	$-1.5\cdot10^{-3}$	$3.5\cdot10^{-5}$
B_0/(MPa)	660	97
B_1/(MPa·K^{-1})	−1.3	0.2
C	0.1	0.01
p_{ref}/MPa	1	
AAD/%	0.04	
MAD/%	0.3	
σ/(kg·m^{-3})	0.7	

where $\rho\left(T,p_{ref}\right)$ represents the reference density, adjusted based on experimental data obtained at a reference pressure of 1 MPa, and it describes the temperature dependence of the fluid density. This density and $B(T)$ function are correlated with polynomial equations as follows:

$$\rho\left(T,p_{ref}\right)=\sum_{i=0}^{2}A_iT^i \tag{37}$$

$$B(T)=\sum_{j=0}^{1}B_jT^j \tag{38}$$

The values of the optimized parameters A_i, B_j and C, along with their standard uncertainties and other statistical parameters as presented in Table 6. Regression analysis was performed using OriginPro software to implement a linear fit for the $B(T)$ function, rather than employing the standard second-order equation. The standard uncertainties of the fitted parameters were calculated as the square roots of the diagonal elements of the variance-covariance matrix $C=(J^TJ)^{-1}\cdot s^2$, where J is the matrix of partial derivatives (Jacobian) and s^2 is the mean residual variance.

4.2. N_2O solubility

Measurements of N_2O solubility in an aqueous mixture of DMAE (30% wt.) and MAPA (10% wt.) were conducted at pressures between (1.4 and 4.5) MPa and at four temperatures: 313.15, 333.15, 363.15 and 393.15 K. The experimental results are reported in Table 7 where molalities are based upon ternary mixture as the solvent and x_{N_2O} denotes the mole fraction of N_2O.

Fig. 3 shows the solubility data expressed as the molality of N_2O in the aqueous ternary mixture of amine as a function of $\left(p-p_s^{sat}\right)$. The solubility data were plotted for four temperatures: 313.15, 333.15 K, 363.15 K and 393.15 K. N_2O solubility demonstrates a typical linear dependence on its partial pressure but decreases significantly with increasing temperature. For instance, at approximately 3 MPa N_2O partial pressure, solubility is reduced by up to 22% between 313.15 and 393.15 K. The solubilities at $T=363.15$ K and $T=393.15$ K are quite similar, suggesting that the intermolecular interactions are significantly weakened and that the gas is approaching a minimum practical solubility at temperatures higher than 363.15 K. This study provides the first data on N_2O solubility in a ternary aqueous amine mixture with MAPA and DMAE under conditions relevant to CO_2 capture.

The regression method used to correlate the experimental data of N_2O solubility, shows a good agreement for the four temperatures evaluated (Fig. 4). For each temperature, the $\ln\left(\hat{f}_{N_2O}/b_{N_2O}\right)$ values are relatively constant across the range of $\left(p-p_s^{sat}\right)$. This indicates that the Henry's law constant is independent of the partial pressure of N_2O at least for this range of pressure ($p<5$ MPa). The slight slope suggests minor non-ideal behaviour, but the dominant trend is linearity.

Fig. 5 shows the Henry's constant of N_2O in pure water and aqueous amine solutions. It reveals that N_2O solubility is dependent on solvent type and temperature. While N_2O solubility decreases as temperatures rises in all systems, the Henry's constant for aqueous MEA (30% wt.) is very similar to pure water. However, amine mixtures of MAPA with DEEA, DMAE and 1-(2-hydroxyethyl)pyrrolidine (1-(2HE)PRLD) dissolve more N_2O than pure water and MEA, especially at $T>313.15$ K. These differences can be explained by how amine molecules arrange themselves in the liquid, which affects the open space available for the gas [46]. Hamza et al. [52] reported that aliphatic compounds can hold more gas than cyclic ones. However, for amines this is not the only factor, as solubility can also be improved if the compound is large, for example, DEEA with its two ethyl groups compared to DMAE with two methyl groups attached to the nitrogen. This shows that the size and shape of these groups make a difference in how molecules pack and how they form hydrogen bonds.

The Krichevsky-Ilinskaya (KI) equation parameters were obtained for each temperature, and the Margules parameters (A) were optimized (Table 8). As described by Carroll and Mather [53], in a linear equation like KI, competing effects can cancel each other out. Specifically, terms related to the partial molar volume at infinite dilution and activity coefficients. This is another reason why the calculation of $\bar{v}^{\infty}_{N_2O}$ is considered independent, assuming its similarity with $\bar{v}^{\infty}_{CO_2}$ in water [38]. Fig. 6 shows that the activity coefficient of N_2O decreases with pressure because it is a function of composition. The Poynting factor shows opposite behaviour, as it is an increasing function of $\bar{v}^{\infty}_{N_2O}$ if this value is positive. The product of both terms represents the overall non-ideality of the gas in the liquid phase.

4.3. Physical CO_2 solubility

The physical solubility of CO_2 in the aqueous amine solution was estimated using the N_2O analogy, a widely employed method for determining the apparent Henry's law constant of CO_2 in liquid systems. N_2O and CO_2 exhibit similar physicochemical properties but N_2O is chemically inert in the presence of amines. This inertness enables the experimental determination of the solubility ratio of N_2O to CO_2 in water, which can then be used to approximate the solubility of CO_2 in the amine solution [54]:

$$H_{CO_2,solution}=\frac{H_{CO_2,water}}{HN_2O,\,water}H_{N_2O,solution}=\frac{1}{R_{H,water}}H_{N_2O,solution} \tag{39}$$

Where $H_{CO_2,water}$ and $H_{N_2O,water}$ are the Henry constant of CO_2 and N_2O in water, respectively. $H_{N_2O,solution}$ is the Henry constant of N_2O experimentally obtained in this work. $R_{H,water}$ is a parameter which depends on the uncertainties of equilibrium data between water-CO_2 and water-N_2O binary systems. For this reason, we use the approach suggested by Monteiro and Svendsen et al. [37] for ($1<p<20$) MPa:

$$R_{H,water}=\exp\left[-6.3231\frac{T_c}{T}+0.3309\left(1-\frac{T}{T_c}\right)^{0.355}\frac{T_c}{T}+5.7203\exp\left(1-\frac{T}{T_c}\right)\left(\frac{T}{T_c}\right)^{-0.41}\right] \tag{40}$$

Table 7
Experimental results of N_2O solubility of an aqueous mixture with DMAE (30% wt.) and MAPA (10% wt.) on N_2O-Free basis. T is temperature, w_{DMAE} is the mass fraction of 2-Dimethylaminoethanol, w_{MAPA} is the mass fraction of N-Methyl-1,3-propanediamine, x_{N_2O} is the mole fraction of N_2O in liquid phase at the given temperature and bubble pressure with standard uncertainty $u(x_{N_2O})$, b_{N_2O} is the molality of N_2O in aqueous amine (mol/kg-solution) at he given temperature and bubble pressure with standard uncertainty $u(b_{N_2O})$, p_b is bubble pressure, $u(p_b)$ is the standard uncertainty of p_b, and p_s^{sat} is the saturation pressure of solvent. [a]

T/K	w_{DMAE} [b]	w_{MAPA} [b]	10^3 x_{N_2O}	10^3 $u(x_{N_2O})$	b_{N_2O}/(mol·kg^{-1})	$u(b_{N_2O})$/(mol·kg^{-1})	p_b/MPa	$u(p_b)$/MPa
p_s^{sat} = 6.73 kPa [c]								
313.18	0.2999	0.0997	5.675	0.025	0.2158	0.0009	1.41	0.17
313.20	0.2999	0.0998	8.179	0.036	0.3118	0.0014	2.08	0.08
313.22	0.2999	0.0997	11.003	0.048	0.4207	0.0018	2.96	0.03
313.20	0.2998	0.0998	13.261	0.058	0.5083	0.0022	3.58	0.09
p_s^{sat} = 18.40 kPa [c]								
333.10	0.2999	0.0998	5.093	0.022	0.1936	0.0008	1.46	0.08
333.09	0.2999	0.0999	8.003	0.035	0.3050	0.0013	2.31	0.05
333.09	0.2999	0.0997	10.401	0.045	0.3975	0.0017	3.09	0.04
333.10	0.2999	0.0998	13.410	0.059	0.5141	0.0022	4.06	0.13
p_s^{sat} = 66.07 kPa [c]								
362.82	0.2999	0.0998	5.756	0.025	0.2189	0.0010	1.84	0.24
362.87	0.2999	0.0998	7.289	0.032	0.2777	0.0012	2.36	0.07
362.84	0.2999	0.0998	9.666	0.042	0.3691	0.0016	3.20	0.11
362.85	0.2999	0.0998	12.434	0.054	0.4761	0.0021	4.11	0.09
p_s^{sat} = 195.55 kPa [d]								
392.63	0.2998	0.0998	4.541	0.020	0.1725	0.0008	1.65	0.06
392.69	0.2999	0.0998	6.842	0.030	0.2605	0.0011	2.40	0.06
392.63	0.2999	0.0998	9.161	0.040	0.3497	0.0015	3.15	0.03
392.65	0.2998	0.0998	12.809	0.056	0.4907	0.0021	4.41	0.12

[a] Standard uncertainty of T is $u(T) = 0.03$ K.
[b] Standard uncertainty of amine mass fraction $u(w_i) = 0.0001$.
[c] Expanded uncertainty in pressure $U(p_s^{sat}) = 0.11$ kPa with a coverage factor of $k = 2$. Values measured with VLE apparatus described in Section 2.5 at $T = 313.15$ K, $T = 333.15$ K, and $T = 363.15$ K.
[d] Assumed to be equal to the saturation pressure of water at mean temperature $T = 392.65$ K and calculated with REFPROP NIST v10.0 database [23].

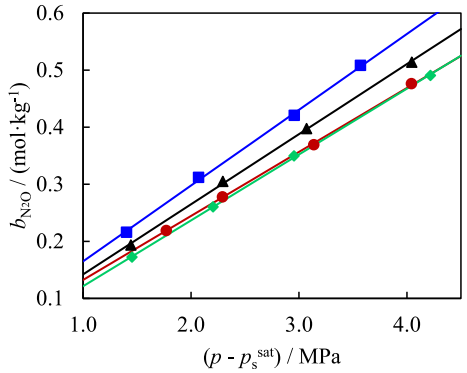

Fig. 3. N_2O solubility, expressed as molality, b_{N_2O} (mol/kg-solution), as a function of the difference between total pressure and saturation pressure of the solvent $(p - p_s^{sat})$. Isotherms: (■) T = 313.15 K, (▲) T = 333.15 K, (●) T = 363.15 K, (◆) T = 393.15 K. Solid lines are calculated from Eqs. (8)–(10).

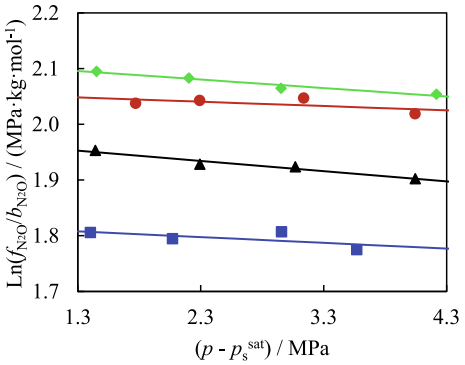

Fig. 4. Plot of $\ln(\hat{f}_{N_2O}/b_{N_2O})$ against $(p - p_s^{sat})$. Isotherms: (■) T = 313.15 K, (▲) T = 333.15 K, (●) T = 363.15 K, (◆) T = 393.15 K. Solid lines are calculated from Eqs. (8)–(10).

where T_c = 647.10 K is the critical temperature of water. Calculated Henry's constants of CO_2 on a molality scale are presented in Table 8.

Rumpf and Maurer [55] calculated the Henry's constant for the solubility of carbon dioxide in pure water, with their data correlated for a temperature range of 273.15 K–473.15 K. As can be seen in Fig. 7, this Henry's constant significantly deviates from that obtained for the ternary aqueous mixture of amine, particularly at temperatures above 313.15 K. For instance, at T = 393.15 K, the Henry's constant in amine-based solvent is approximately 5 MPa·kg·mol^{-1} lower. The real values were adjusted using a polynomial equation of second order:

$$H_{CO_2,c} = \sum_{i=0}^{2} a_i T^i \tag{41}$$

where a_i are adjustable coefficients with their standard uncertainties reported in Table 9.

4.4. Experimental data for CO_2 solubility

Experimental CO_2 solubility data were measured in an aqueous solution of 30% wt. DMAE and 10% wt. MAPA at temperatures of 313.15 K, 333.15 K and 363.15 K and loadings up to 1.3 mol-CO_2/mol-amine. The technique used is described in Section 2.5. These data are presented in Table 10, with their respective expanded relative uncertainties (k = 2).

Fig. 8 presents a comparison of equilibrium data at 313.15 K for the mixture evaluated in this work in relation to other aqueous mixtures with similar compositions containing at least DMAE or MAPA. Given the different molar masses of the pure components, the CO_2 loading indicator (α) should be compared based on the total mass of amine. For instance, the equilibrium data reported by Bernhardsen et al. [8] for the system 3DMA1P (32% wt.) + MAPA (9% wt.), with an average total amine molar mass of 99.72 g/mol, and for the system 1-(2HE)PRLD (34% wt.) + MAPA (9% wt.) equivalent to 108.54 g/mol, suggest a

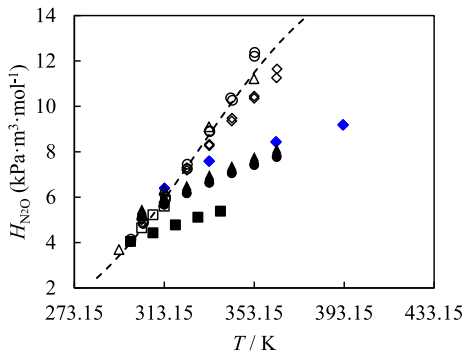

Fig. 5. Henry's constant of N_2O as a function of temperature in pure water and mixed solvents based on amines. Legend: (◆) This work, aqueous mixture with DMAE (30% wt.) and MAPA (10% wt.); (■) Monteiro et al. [13] in aqueous DEEA (~36% wt.) + MAPA (~9% wt.) mixture; (▲) Bernhardsen and Knuutila [46] in aqueous 3DMA1P (31.7% wt.) + MAPA (9% wt.) mixture; (●) Bernhardsen and Knuutila [46] in aqueous 1-(2HE)PRLD (34.4% wt.) + MAPA (8.8% wt.) mixture; (◇) Bernhardsen et al. [47] aqueous MEA (30% wt.) mixture; (□) Ko and Li [48] in pure water; (△) Rinker and Sandall [49] in pure water; (○) Hartono et al. [50] in pure water. Dashed line represents correlated data of Henry's constant of N_2O in pure water from Penttilä et al. [51].

higher CO_2 loading capacity. This is because both mixtures have 0.411 and 0.396 total moles per 100 g of solution, respectively, unlike the mixture evaluated in this study, which has 0.450 mol per 100 g of solution.

Furthermore, when comparing the data of Zoghi et al. [19], it is possible to observe that the loading improves significantly when the mixture composition is changed, reducing the total DMAE concentration to 30% and increasing the amount of MAPA to a mass concentration of 10%, for a total amine of 40% wt. For example, at a partial CO_2 pressure of approximately ~40 kPa, the loading is 0.165 mol-CO_2/mol-amine higher for the mixture in this study. Although the mixture evaluated in this work has 5% wt. less MAPA, both mixtures differ by only 0.056 mol of total amine per 100 g of solution. On the other hand, both DMAE and MAPA have very similar molar masses, 88.89 g/mol and 89.14 g/mol, respectively, so regardless of the changes in the mass distribution of each pure amine in the mixture, the total number of moles do not change significantly. Regarding the system shown by Delavari et al. [6] (40% wt. DMAE +5% wt. EAE), the mixture has up to five times higher loading capacity, for example, at a CO_2 partial pressure of 3.44 kPa. Even though MAPA is commonly used as an absorption activator [56], it can also have a positive effect on loading capacity [57] being a diamine with a primary and secondary amine group, compared to EAE which only has a secondary amino group. Moreover, El Hadri et al. [58] state that the positive effect of DMAE in the mixture is due to the two methyl functional groups in its structure that act as electron donors, which is beneficial for increasing CO_2 absorption capacity as shown in Fig. 9.

4.5. Modelling results for CO_2 solubility

The VLE data for CO_2 solubility in the aqueous amine blend were fitted using an empirical correlation, soft-model proposed by Brúder et al. [62] without thermodynamic significance and also used by other authors [8]. This model correlates CO_2 partial pressure with

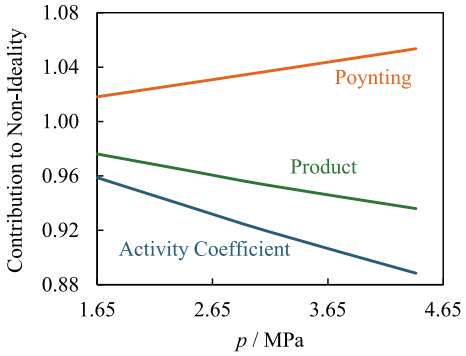

Fig. 6. Liquid phase non-idealities of N_2O for the aqueous mixture with DMAE (30% wt.) and MAPA (10% wt.) evaluated in this work at $T = 393.15$ K.

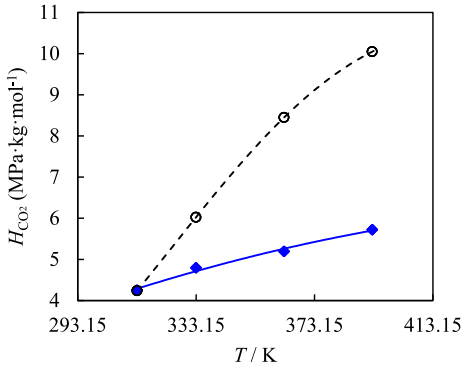

Fig. 7. Henry's constant of CO_2 as a function of temperature obtained from this work (—) for the aqueous mixture with DMAE (30% wt.) + MAPA (10% wt.) and Henry's constant of CO_2 in pure water: (○,- - -) Rumpf and Maurer [55]. Dashed line represents correlated data of Henry's constant of CO_2 in pure water. Solid line represents adjusted values of Henry's constant of CO_2 (Eq. (41)).

Table 9
Correlated coefficients to calculate the Henry's constant of CO_2 ($H_{CO_2,c}$) in the aqueous mixture with DMAE (30% wt.) and MAPA (10% wt.). Standard deviations σ, absolute average deviation (AAD) and maximum average deviation (MAD) for Eq. (41).

Coefficient	Value	Standard uncertainty	Unit
a_0	−8.6	3.0	MPa·kg·mol^{-1}
a_1	$6.0\cdot10^{-2}$	$1.7\cdot10^{-2}$	MPa·kg·mol^{-1}·K^{-1}
a_2	$-6.0\cdot10^{-5}$	$2.4\cdot10^{-5}$	MPa·kg·mol^{-1}·K^{-2}
AAD/%	1		
MAD/%	1.7		
σ/(MPa·kg·mol^{-1})	0.12		

Table 8
Parameters of the Krichevsky-Ilinskaya Equation and estimated Henry's constant of N_2O and CO_2.

T/K	$\bar{v}^{\infty}_{N_2O}$/ cm^3·mol^{-1}	A/RT	$R_{H,water}$	$H_{N_2O,solution}$/ MPa·kg·mol^{-1}	[a] $H_{CO_2,solution}$/ MPa·kg·mol^{-1}	[b] $H_{CO_2,c}$/ MPa·kg·mol^{-1}
313.15	33.40	3.38	1.46	6.218	4.250	4.287
333.15	34.70	4.90	1.51	7.263	4.797	4.714
363.15	37.18	3.46	1.52	7.866	5.192	5.265
393.15	40.34	4.65	1.45	8.314	5.722	5.707

[a] Calculated from Eqs. (39)–(40).
[b] Calculated from Eq. (41).

Table 10
Experimental solubility of CO_2, α_{exp} (mol-CO_2/mol-amine), in the aqueous 30% wt. DMAE +10% wt. MAPA solution and its corresponding expanded uncertainty, $U(\alpha_{exp})$. T is temperature, p is the total pressure, p_{CO_2} is the CO_2 partial pressure and w_i is the mass fraction of amine in aqueous mixture. Calculated values of CO_2 partial pressure $\left(p_{CO_2,c}\right)$ with soft-model (Eqs. (42)–(45)) and of CO_2 loading (α_c) with $\gamma-\phi$ model (Eqs. (18)–(31)).

p/kPa[a]	p_{CO_2}/kPa	α_{exp}	$U(\alpha_{exp})$[b]	$U_r(\alpha_{exp})$[b]	$p_{CO_2,c}$/kPa	α_c
$T = 313.15$ K[d], $w_{DMAE} = 0.2996$[c], $w_{MAPA} = 0.0998$[c]						
6.73		0				
8.16	1.43	0.399	0.003	0.7%	1.34	0.419
10.17	3.44	0.498	0.003	0.7%	3.26	0.499
14.15	7.42	0.599	0.004	0.7%	6.99	0.601
30.23	23.50	0.745	0.005	0.7%	20.67	0.761
46.63	39.90	0.817	0.005	0.7%	38.60	0.828
82.63	75.90	0.884	0.006	0.7%	77.04	0.893
150.43	143.70	0.941	0.006	0.7%	152.45	0.940
321.7	315.0	1.004	0.007	0.7%	337.2	0.990
783.8	777.1	1.071	0.010	0.9%	802.2	1.064
1448.3	1441.6	1.123	0.016	1.4%	1492.5	1.120
2295.7	2289.0	1.169	0.025	2.2%	2444.5	1.164
3322.7	3316.0	1.207	0.039	3.2%	3528.5	1.204
4897.2	4890.5	1.245	0.066	5.3%	4870.4	1.247
7055.7	7049.0	1.283	0.123	9.6%	6546.3	1.276
$T = 333.15$ K[d], $w_{DMAE} = 0.2996$[c], $w_{MAPA} = 0.0997$[c]						
18.40		0				
22.62	4.22	0.401	0.003	0.7%	5.44	0.382
29.29	10.89	0.499	0.003	0.7%	13.01	0.486
45.24	26.84	0.599	0.004	0.7%	27.55	0.598
55.25	36.85	0.650	0.004	0.7%	39.43	0.641
89.76	71.36	0.739	0.005	0.7%	72.92	0.734
137.29	118.89	0.808	0.005	0.7%	121.32	0.806
223.4	205.0	0.877	0.006	0.7%	211.7	0.876
396.7	378.3	0.935	0.007	0.7%	361.4	0.942
795.9	777.5	0.999	0.009	0.9%	693.0	1.008
1694.8	1676.4	1.067	0.016	1.5%	1438.9	1.076
3411.7	3393.3	1.137	0.034	3.0%	3111.4	1.147
6527.7	6509.3	1.201	0.081	6.7%	6153.0	1.200
$T = 363.15$ K[d], $w_{DMAE} = 0.2999$[c], $w_{MAPA} = 0.0997$[c]						
66.07		0				
76.07	10.00	0.301	0.002	0.7%	10.39	0.293
103.03	36.96	0.399	0.003	0.7%	31.95	0.419
126.50	60.43	0.453	0.003	0.7%	52.93	0.468
153.12	87.05	0.504	0.003	0.7%	80.84	0.509
189.2	123.2	0.552	0.004	0.7%	117.2	0.550
236.6	170.6	0.601	0.004	0.7%	166.9	0.594
299.6	233.6	0.651	0.004	0.7%	235.5	0.640
391.9	325.9	0.704	0.005	0.7%	335.1	0.693
519.7	453.7	0.756	0.006	0.7%	472.3	0.748
697.7	631.7	0.806	0.007	0.8%	656.5	0.802
943.2	877.2	0.854	0.008	0.9%	910.5	0.852
1375.5	1309.5	0.907	0.011	1.2%	1327.8	0.906
2140.6	2074.6	0.965	0.016	1.7%	2055.9	0.959
3576.6	3510.6	1.029	0.029	2.8%	3429.2	1.028
5123.8	5057.8	1.078	0.045	4.2%	5137.9	1.082
6877.4	6811.4	1.130	0.067	5.9%	8104.4	1.125

[a] Expanded uncertainty in pressure $U(p) = 0.11$ kPa for $p < 160$ kPa and $U(p) = 2.8$ kPa for $p > 160$ kPa reported with a coverage factor of $k = 2$.
[b] Expanded uncertainty in CO_2 loading $U(\alpha)$ reported with a coverage factor of $k = 2$.
[c] Standard uncertainty of amine mass fraction $u(w_i) = 0.0001$.
[d] Standard uncertainty of temperature $u(T) = 0.02$ K.

temperature and CO_2 loading, since solubility is commonly represented in this way, thus allowing its use to be extended to other aqueous amine-based systems. It should be noted that the coefficients derived from this correlation are specific to the system evaluated in this work, and its validity is restricted to the studied composition and temperature range. Despite its simplicity, it proves valuable for estimating other properties, such as the heat of absorption, with minimal deviation from experimental data:

$$\ln\left(p_{CO_2}/\text{kPa}\right) = A\ln\alpha + k_1 + B(1 + k_2 exp(-k_3\ln\alpha))^{-1} \quad (42)$$

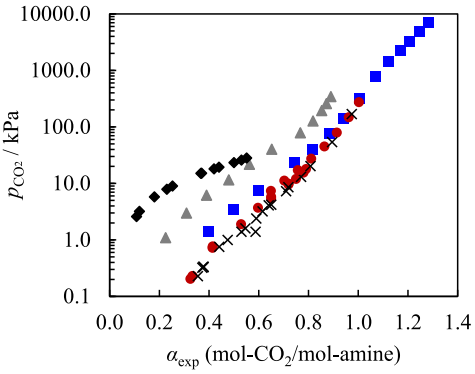

Fig. 8. Solubility of CO_2, expressed as CO_2 partial pressure (p_{CO2}) as a function of CO_2 loading (α_{exp}), in different types of aqueous amines solutions with DMAE or MAPA at $T = 313.15$ K. Legend: (■) This work, 30% wt. DMAE +10% wt. MAPA; (◆) Delavari et al. [6], 40% wt. DMAE +5% wt. EAE; (▲) Zoghi et al. [19], 40% wt. DMAE +5% wt. MAPA; (✖) Bernhardsen et al. [8], 34% wt. 1-(2HE)PRLD +9% wt. MAPA; (●) Bernhardsen et al. [8], 32% wt. 3DMA1P + 9% wt. MAPA.

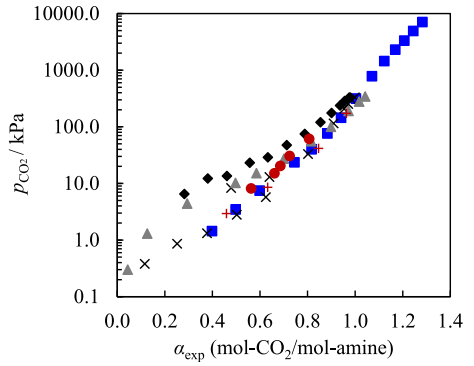

Fig. 9. Solubility of CO_2, expressed as CO_2 partial pressure (p_{CO2}) as a function of CO_2 loading (α_{exp}), in aqueous amines solutions with DMAE at $T = 313.15$ K from different literature sources in comparison to the system studied in this work. Legend: (■) This work, 30% wt. DMAE +10% wt. MAPA; (◆) Tong et al. [59], ~36% wt. (4 M) DMAE; (▲) Tong et al. [59], ~23% wt. (2.5 M) DMAE; (✖) Tong et al. [59], ~9% wt. (1 M) DMAE; (●) Xiao et al. [60], 18.1% wt. DMAE; (+) Liu et al. [61], ~23% wt. (2.5 M) DMAE.

Table 11
Parameters for the CO_2 partial pressure correlation given in Eqs. (42)–(45) with standard deviations σ, absolute average deviation (AAD) and maximum average deviation (MAD).

Parameters	Value	Standard uncertainty
A	3.9	$2.3\cdot10^{-1}$
B	4.7	$6.5\cdot10^{-1}$
k_{11}	$2.7\cdot10^{1}$	$5.4\cdot10^{-1}$
k_{12}	$7.2\cdot10^{3}$	$1.5\cdot10^{2}$
k_{21}	$1.2\cdot10^{6}$	$2.4\cdot10^{5}$
k_{22}	$3.7\cdot10^{8}$	$7.6\cdot10^{7}$
k_{31}	$-3.8\cdot10^{3}$	$1.8\cdot10^{3}$
k_{32}	$-1.7\cdot10^{2}$	8.5
k_{33}	$-2.6\cdot10^{1}$	1.1
AAD/%	2.1	
MAD/%	18	
$\sigma(\ln(p_{CO_2}/\text{kPa}))$	0.1	

$$k_1 = k_{11} - k_{12}/T \quad (43)$$

$$k_2 = exp(k_{21}/T^2 - k_{22}/T^3) \quad (44)$$

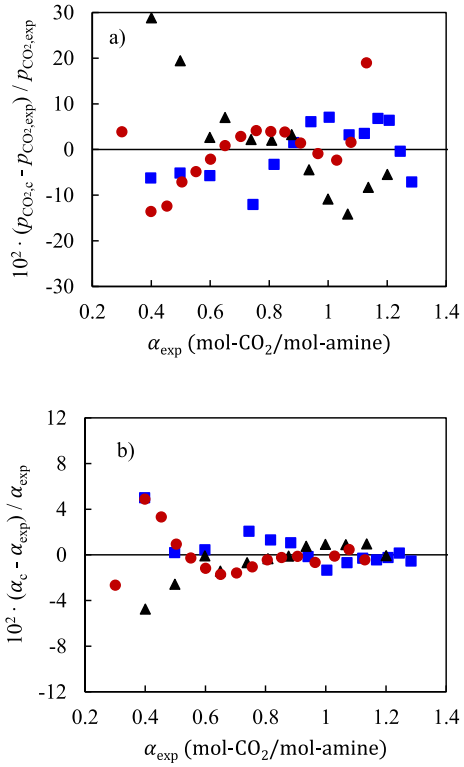

Fig. 10. Relative deviations (%) of: (a) calculated CO_2 partial pressures and (b) calculated CO_2 loadings from experimental data, using the soft-model and thermodynamic $\gamma - \phi$ model, respectively. Legend: (■) $T = 313.15$ K, (▲) $T = 333.15$ K, (▲) $T = 363.15$ K.

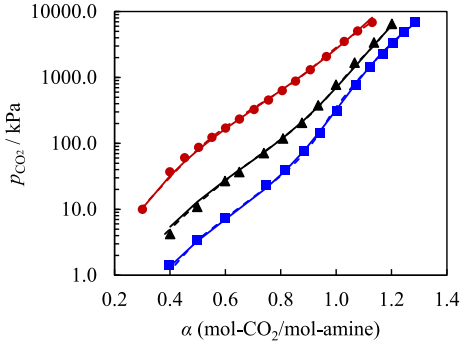

Fig. 11. Experimental data of CO_2 solubility in the aqueous solution of 30% wt. DMAE +10% wt. MAPA at: (■) $T = 313.15$ K, (▲) $T = 333.15$ K, (●) $T = 363.15$ K. Solid lines: soft-model; dashed lines: thermodynamic $\gamma - \phi$ (model)

$$k_3 = k_{31}/T - k_{32} + k_{33}\ln T \tag{45}$$

where A, B and k_i are adjustable parameters which are shown in Table 11.

Fig. 10a shows the relative deviations obtained using the soft-model. The correlation provides an AAD of 6.4% and a MAD of 29% for the CO_2 partial pressure, with deviations that appear random and independent of the CO_2 loading range. In contrast, the thermodynamic model tends to overestimate its value at low loadings and low temperatures (Fig. 10b). Nevertheless, the Deshmuk-Mather model accurately reproduces the solubility data with good precision (AAD = 1.1%) providing better results for the CO_2 capture relevant loading range ($\alpha > 0.5$ mol-CO_2/mol-amine). While both approaches reasonably represent the experimental data (Fig. 11), the empirical equation can be particularly useful due to its simplicity and fast optimization compared to the more complex $\gamma - \phi$

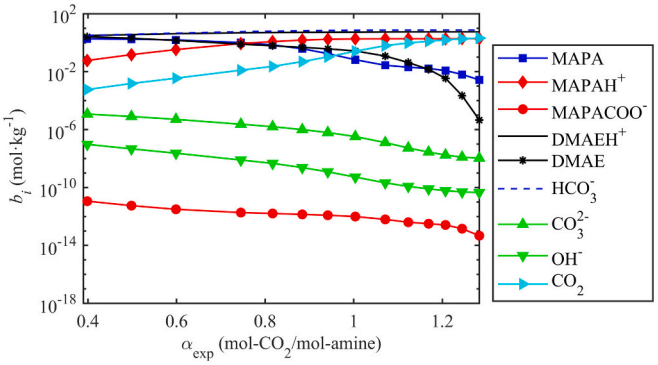

Fig. 12. Distribution of species in the aqueous solution of 30% wt. DMAE +10% wt. MAPA at $T = 313.15$ K. Molality, b_i, expressed as mol per kg of water.

model. The main strength of the D-M framework lies in its rigorous thermodynamic basis and its ability to describe reaction equilibria and non-idealities in aqueous amine systems [40–44]. Although the D-M model is formally general, the fitted interaction parameters and equilibrium constants obtained here are not generalizable. They are specific to the DMAE + MAPA + H_2O blend at the studied composition and temperature range. In this work, 12 liquid-phase species and 19 binary interaction parameters were considered; this formulation provides a consistent basis for describing this tertiary-amine/diamine system, but the numerical values of the optimized parameters cannot be directly transferred to other amine mixtures.

The species and their molal concentrations in the liquid phase are shown in Fig. 12. As demonstrated by Zoghi et al. [19] for a similar system, the concentrations of MAPA and DMAE decrease as the CO_2 loading increases. Conversely, the concentrations of protonated DMAE and HCO_3^- increase with loading, becoming the dominant species in the liquid phase. The reversion of the MAPA carbamate is also observed, along with low concentrations of other species such as diprotonated MAPA (not shown due to low concentration), CO_3^{2-}, and OH^-. Unlike aqueous mixtures of primary or secondary amines, which have a stoichiometric loading capacity limit of 0.5 mol-CO_2/mol-amine [63], the mixture evaluated in this study, containing a tertiary amine (DMAE), allow for loadings greater than this limit, even approaching 1 mol-CO_2/mol-amine. It is also evident that the concentration and physical solubility of CO_2 become significant at high loadings, highlighting the importance of accurately modelling the Henry's law constant for CO_2. Concentrations in the liquid phase are expressed on a molality basis (mol per kg of water), consistent with the electrolyte thermodynamic framework employed. As the solvent consists of water and amines, normalization with respect to water alone may yield numerically large concentration values. For instance, at $T = 313.15$ K, p_{CO_2}=7049 kPa and a CO_2-loading of 1.281 mol-CO_2/mol-amine, the predicted physically dissolved CO_2 concentration of 2 mol/kg-H_2O corresponds to a mole fraction in the solution of approximately 0.03 mol-CO_2/mol-solution.

The thermodynamic model allows the calculation of activity coefficients for predominant species present in the liquid phase. In particular, the activity coefficient of CO_2 is used to determine the physical CO_2 loading in the mixture, thereby accounting for the corrections associated with non-ideality (Eq. (30)). These corrections include the CO_2 fugacity coefficient, the real Henry's constant for the evaluated mixture, and the Poynting factor. Since physical solubility is expressed on a molality basis, b_{CO_2} (mol/kg-H_2O), the physical loading is defined as follows:

$$\alpha_p \left[\frac{\text{mol} - CO_2}{\text{mol} - \text{amine}}\right] = b_{CO_2} \cdot w_{H_2O} \cdot \left(\frac{M_{DMAE} M_{MAPA}}{w_{DMAE} M_{MAPA} + w_{MAPA} M_{DMAE}}\right) \tag{46}$$

where M_i is the molar mass and w_i is the mass fraction of component i. Fig. 13 shows that the contribution of physical CO_2 solubility relative to

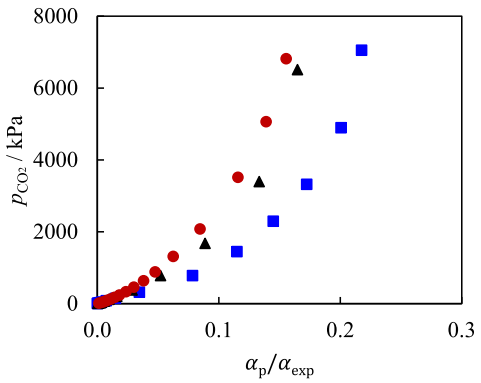

Fig. 13. Ratio between physical (α_p) and total CO_2 loading (α_{exp}) at: (■) T = 313.15 K, (▲) T = 333.15 K, (●) T = 363.15 K.

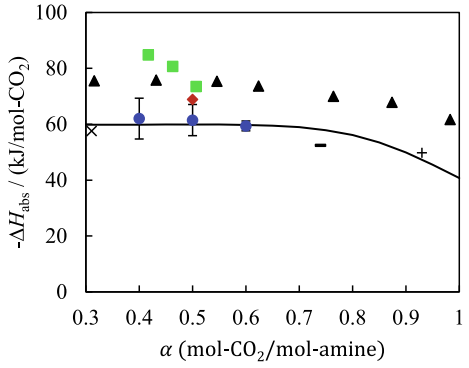

Fig. 14. Heat of CO_2 absorption as a function of CO_2 loading: (●). This work, 30% wt. DMAE +10% wt. MAPA; (■) Kim et al. [64], 30% wt. MEA; (✖) Arcis et al. [65], 30% wt. MDEA; (−) Hadri et al. [58], 30% wt. MDEA; (+) Kierzkowska-Pawlak [66], 30% wt. MDEA; (◆) Chowdhury et al. [67], 30% wt. DEA; (▲) Arcis et al. [68], 30% wt. AMP. Solid line: soft-model.

the total solubility increases with increasing CO_2 partial pressure, indicating that physical absorption becomes more relevant at higher pressures.

4.6. Heat of CO_2 absorption

The heats of absorption, $-\Delta H_{abs}$ (kJ/mol-CO_2), of the aqueous solution with 30% wt. DMAE +10% wt. MAPA were calculated using the soft-model (Fig. 14), based on phase-equilibrium data and the following thermodynamic equation:

$$\left[\frac{\partial(\ln p_{CO_2})}{\partial\left(\frac{1}{T}\right)}\right]_{\alpha} = -\frac{\Delta H_{abs}}{R} \tag{47}$$

where R represents the universal gas constants 8.314 (kJ·kmol^{-1}·K^{-1}). Moreover, $-\Delta H_{abs}$ were estimated from the equilibrium data at loadings close to 0.4, 0.5 and 0.6 mol-CO_2/mol-amine, yielding 62.02 ± 7.30, 61.49 ± 5.58 and 59.41 ± 1.76 kJ/mol-CO_2, respectively. The observed decrease in the heat of absorption with increasing CO_2 loading is consistent with progressive saturation of amine reactive sites and the larger contribution of physical absorption at higher loadings.

Alkanolamine systems such as MEA, DEA and AMP show heats of absorption between 70 and 90 kJ/mol-CO_2 for 30% wt. aqueous solutions, whereas the system evaluated in this work shows significantly lower values. In contrast, the results are comparable to those reported for MDEA. Although MAPA is a potentially good absorbent for improving both the absorption rate and capacity, DMAE is effective at reducing the heat of CO_2 absorption. The relatively small standard uncertainties (≤ 7.30 kJ/mol-CO_2) confirm that the estimated values are consistent with the linear regression of the equilibrium data.

5. Conclusions

This work presents novel density data of the DMAE (30% wt.) + MAPA (10% wt.) + H_2O (60% wt.) system over a wide range of temperatures and pressures and a consistent thermodynamic basis for the analysis of high-pressure phase equilibria relevant to CO_2 capture.

N_2O solubility measurements enabled the determination of the real Henry's law constant of CO_2 in the aqueous amine mixture. The results highlight the significant deviation of physical CO_2 solubility in amine-water systems compared to pure water. This pronounced deviation evidences the strong influence of amine-water interactions on gas dissolution behaviour and provides key parameters for rigorous thermodynamic modelling of reactive absorption systems. The results also highlight that gas solubility is strongly dependent on the nature and structure of the amine molecules. Mixtures of amines with larger or more alkyl groups show enhanced gas solubility than single amines, particularly at elevated temperatures. This reflects the influence of molecular size, shape and hydrogen-bonding interactions on solvent packing and gas accommodation.

New Vapour-Liquid Equilibrium (VLE) data for CO_2 were obtained for this blended amine system. These results were successfully correlated using a thermodynamic $\gamma - \phi$ model, achieving an excellent agreement with the experimental data (AAD = 1.1%). The heat of absorption was calculated based on the empirical soft-model, which effectively reproduced the natural logarithm of the equilibrium partial pressures of CO_2, with a low relative deviation from experimental measurements (AAD = 2.1%). A comparison of this property with conventional simple amines demonstrated that the studied aqueous amine system shows a lower heat of absorption, suggesting a reduced energy penalty for regeneration in industrial-scale applications. Overall, these findings advance the thermodynamic understanding of blended amine systems and support the development of more energy-efficient CO_2 capture solvents.

CRediT authorship contribution statement

Juan D. Arroyave: Writing – review & editing, Writing – original draft, Methodology, Investigation, Formal analysis, Data curation. **Alejandro Moreau:** Writing – review & editing, Validation, Supervision, Methodology, Formal analysis, Conceptualization. **Xavier Paredes:** Writing – review & editing, Validation, Supervision, Methodology, Formal analysis, Conceptualization. **Fredy Vélez:** Writing – review & editing, Validation, Formal analysis. **J.P. Martin Trusler:** Writing – review & editing, Validation, Supervision, Methodology, Formal analysis. **M. Carmen Martín:** Writing – review & editing, Validation, Supervision, Project administration, Methodology, Funding acquisition, Formal analysis, Conceptualization.

Declaration of competing interest

The authors declare that they have no known competing financial interests or personal relationships that could have appeared to influence the work reported in this paper.

Acknowledgements

Juan D. Arroyave has been funded by the call for predoctoral contracts UVa 2021. This work is part of grant PID2021-125749OB-I00 funded by MICIU/AEI/10.13039/501100011033 and by ERDF/EU. Financial support of the Department of Education of the Junta de Castilla y León and FEDER Funds is gratefully acknowledged (Reference: CLU-2025-2-05, Unidad de Excelencia BioecoUVa, Universidad de Valladolid).

Data availability

Data will be made available on request.

References

[1] Z. (Henry) Liang, W. Rongwong, H. Liu, K. Fu, H. Gao, F. Cao, R. Zhang, T. Sema, A. Henni, K. Sumon, D. Nath, D. Gelowitz, W. Srisang, C. Saiwan, A. Benamor, M. Al-Marri, H. Shi, T. Supap, C. Chan, Q. Zhou, M. Abu-Zahra, M. Wilson, W. Olson, R. Idem, P.(P.T) Tontiwachwuthikul, Recent progress and new developments in post-combustion carbon-capture technology with amine based solvents, Int. J. Greenhouse Gas Control 40 (2015) 26–54, https://doi.org/10.1016/j.ijggc.2015.06.017.

[2] S.A. Mazari, L. Ghalib, A. Sattar, M.M. Bozdar, A. Qayoom, I. Ahmed, A. Muhammad, R. Abro, A. Abdulkareem, S. Nizamuddin, H. Baloch, N. M. Mubarak, Review of modelling and simulation strategies for evaluating corrosive behavior of aqueous amine systems for CO2 capture, Int. J. Greenh. Gas Con. 96 (2020) 103010, https://doi.org/10.1016/j.ijggc.2020.103010.

[3] J. Du, W. Yang, L. Xu, L. Bei, S. Lei, W. Li, H. Liu, B. Wang, L. Sun, Review on post-combustion CO2 capture by amine blended solvents and aqueous ammonia, Chem. Eng. J. 488 (2024) 150954, https://doi.org/10.1016/j.cej.2024.150954.

[4] A. Henni, J. Li, P. Tontiwachwuthikul, Reaction kinetics of CO2 in aqueous 1-amino-2-propanol, 3-amino-1-propanol, and dimethylmonoethanolamine solutions in the temperature range of 298-313 k using the stopped-flow technique, Ind. Eng. Chem. Res. 47 (2008) 2213–2220, https://doi.org/10.1021/ie070587r.

[5] W. Conway, S. Bruggink, Y. Beyad, W. Luo, I. Melián-Cabrera, G. Puxty, P. Feron, CO2 absorption into aqueous amine blended solutions containing monoethanolamine (MEA), N,N-dimethylethanolamine (DMEA), N,N-diethylethanolamine (DEEA) and 2-amino-2-methyl-1-propanol (AMP) for post-combustion capture processes, Chem. Eng. Sci. 126 (2015) 446–454, https://doi.org/10.1016/j.ces.2014.12.053.

[6] M. Delavari, M. Khajenoori, A.T. Zoghi, Equilibrium absorption of CO2 in aqueous solution of n-dimethylamino ethanol and 2-(ethylamino)ethanol, measuring and thermodynamic modeling, J. Chem. Thermodyn. 186 (2023) 107142, https://doi.org/10.1016/j.jct.2023.107142.

[7] B. Aghel, S. Janati, S. Wongwises, M. Safdari, Review on CO2 capture by blended amine solutions, Int. J. Greenh. Gas Con. 119 (2022) 103715, https://doi.org/10.1016/j.ijggc.2022.103715.

[8] I.M. Bernhardsen, A.A. Trollebø, C. Perinu, H.K. Knuutila, Vapour-liquid equilibrium study of tertiary amines, single and in blend with 3-(methylamino) propylamine, for post-combustion CO2 capture, J. Chem. Thermodyn. 138 (2019) 211–228, https://doi.org/10.1016/j.jct.2019.06.017.

[9] S.Y. Choi, S.C. Nam, Y. Il Yoon, K.T. Park, S.J. Park, Carbon dioxide absorption into aqueous blends of methyldiethanolamine (MDEA) and alkyl amines containing multiple amino groups, Ind. Eng. Chem. Res. 53 (2014) 14451–14461, https://doi.org/10.1021/ie502434m.

[10] M. Garcia, H.K. Knuutila, S. Gu, Determination of kinetics of CO2 absorption in unloaded and loaded DEEA+MAPA blend, Energy Proc. 114 (2017) 1772–1784. Elsevier Ltd, https://doi.org/10.1016/j.egypro.2017.03.1305.

[11] E. Kruszczak, H. Kierzkowska-Pawlak, CO2 capture by absorption in activated aqueous solutions of N,N-Diethylethanoloamine, Ecol. Chem. Eng. S 24 (2017) 239–248, https://doi.org/10.1515/eces-2017-0016.

[12] D.D.D. Pinto, S.A.H. Zaidy, A. Hartono, H.F. Svendsen, Evaluation of a phase change solvent for CO2 capture: absorption and desorption tests, Int. J. Greenh. Gas Con. 28 (2014) 318–327, https://doi.org/10.1016/j.ijggc.2014.07.002.

[13] J.G.M.S. Monteiro, H. Majeed, H. Knuutila, H.F. Svendsen, Kinetics of CO2 absorption in aqueous blends of N,N-diethylethanolamine (DEEA) and N-methyl-1,3-propane-diamine (MAPA), Chem. Eng. Sci. 129 (2015) 145–155, https://doi.org/10.1016/j.ces.2015.02.001.

[14] H.K. Knuutila, Å. Nannestad, Effect of the concentration of MAPA on the heat of absorption of CO2 and on the cyclic capacity in DEEA-MAPA blends, Int. J. Greenh. Gas Con. 61 (2017) 94–103, https://doi.org/10.1016/j.ijggc.2017.03.026.

[15] M.W. Arshad, P.L. Fosbøl, N. Von Solms, H.F. Svendsen, K. Thomsen, Heat of absorption of CO2 in phase change solvents: 2-(diethylamino)ethanol and 3-(methylamino)propylamine, J. Chem. Eng. Data 58 (2013) 1974–1988, https://doi.org/10.1021/je400289v.

[16] P. Brúder, K.G. Lauritsen, T. Mejdell, H.F. Svendsen, CO2 capture into aqueous solutions of 3-methylaminopropylamine activated dimethyl-monoethanolamine, Chem. Eng. Sci. 75 (2012) 28–37, https://doi.org/10.1016/j.ces.2012.03.005.

[17] P. Brúder, F. Owrang, H.F. Svendsen, Pilot study-CO2 capture into aqueous solutions of 3-methylaminopropylamine (MAPA) activated dimethyl-monoethanolamine (DMMEA), Int. J. Greenh. Gas Con. 11 (2012) 98–109, https://doi.org/10.1016/j.ijggc.2012.07.004.

[18] A. Rahimi, A.T. Zoghi, F. Feyzi, A.H. Jalili, Experimental study of density, viscosity and equilibrium carbon dioxide solubility in some aqueous alkanolamine solutions, J. Solution Chem. 48 (2019) 489–501, https://doi.org/10.1007/s10953-019-00872-4.

[19] A.T. Zoghi, A. Rahimi, F. Feyzi, A.H. Jalili, Measuring and modeling equilibrium solubility of carbon dioxide in aqueous solution of dimethylaminoethanol and 3-methylaminopropylamine, Thermochim. Acta 686 (2020) 178565, https://doi.org/10.1016/j.tca.2020.178565.

[20] J.J. Segovia, O. Fandiño, E.R. López, L. Lugo, M. Carmen Martín, J. Fernández, Automated densimetric system: measurements and uncertainties for compressed fluids, J. Chem. Thermodyn. 41 (2009) 632–638, https://doi.org/10.1016/j.jct.2008.12.020.

[21] JCGM 100:2008, Evaluation of measurement data - Guide to the expression of uncertainty in measurement, 2008. http://www.bipm.org/en/publications/guides/gum.html.

[22] W. Wagner, A. Pruß, The IAPWS formulation 1995 for the thermodynamic properties of ordinary water substance for general and scientific use, J. Phys. Chem. Ref. Data 31 (2002) 387–535, https://doi.org/10.1063/1.1461829.

[23] E.W. Lemmon, I.H. Bell, M.L. Huber, M.O. McLinden, NIST Standard Reference Database 23: Reference Fluid Thermodynamic and Transport Properties-REFPROP, Version 10.0, National Institute of Standards and Technology, 2018, https://doi.org/10.18434/T4/1502528.

[24] B. Lagourette, C. Boned, H. Saint-Guirons, P. Xans, H. Zhou, Densimeter calibration method versus temperature and pressure, Meas. Sci. Technol. 3 (1992) 699–703, https://doi.org/10.1088/0957-0233/3/8/002.

[25] M.J.P. Comuñas, J.-P. Bazile, A. Baylaucq, C. Boned, Density of diethyl adipate using a new vibrating tube densimeter from (293.15 to 403.15) k and up to 140 MPa. Calibration and measurements, J. Chem. Eng. Data 53 (2008) 986–994, https://doi.org/10.1021/je700737c.

[26] G.A. Torín-Ollarves, J.P.M. Trusler, Solubility of hydrogen in sodium chloride brine at high pressures, Fluid Phase Equilib. 539 (2021) 113025, https://doi.org/10.1016/j.fluid.2021.113025.

[27] Q. Chen, J.P.M. Trusler, Solubility of CO in water and NaCl(aq) at high pressures, Chem. Eng. Sci. 293 (2024) 120038, https://doi.org/10.1016/j.ces.2024.120038.

[28] G. Kling, G. Maurer, The solubility of hydrogen in water and in 2-aminoethanol at temperatures between 323 k and 423 k and pressures up to 16 m pa, J. Chem. Thermodyn. 23 (1991) 531–541, https://doi.org/10.1016/S0021-9614(05)80095-3.

[29] R.E. Gibbs, H.C. Van Ness, Vapor—Liquid equilibria from total-pressure measurements. a new apparatus, Ind. Eng. Chem. Fundam. 11 (1972) 410–413, https://doi.org/10.1021/i160043a022.

[30] R. Span, W. Wagner, A new equation of state for carbon dioxide covering the fluid region from the triple-point temperature to 1100 k at pressures up to 800 MPa, J. Phys. Chem. Ref. Data Monogr. 25 (1996) 1509–1596, https://doi.org/10.1063/1.555991.

[31] F.-Y. Jou, A.E. Mather, F.D. Otto, The solubility of CO2 in a 30 mass percent monoethanolamine solution, Can. J. Chem. Eng. 73 (1995) 140–147, https://doi.org/10.1002/cjce.5450730116.

[32] D. Tong, J.P.M. Trusler, G.C. Maitland, J. Gibbins, P.S. Fennell, Solubility of carbon dioxide in aqueous solution of monoethanolamine or 2-amino-2-methyl-1-propanol: experimental measurements and modelling, Int. J. Greenh. Gas Con. 6 (2012) 37–47, https://doi.org/10.1016/j.ijggc.2011.11.005.

[33] L. Feng, D. Zheng, W. Huang, Sync-measurement experimental study of (fluoroethane + dimethylether tetraethylene glycol), (fluoroethane + dimethylether triethylene glycol) and (fluoroethane + dimethylether diethylene glycol) systems, J. Chem. Thermodyn. 98 (2016) 149–158, https://doi.org/10.1016/j.jct.2016.03.015.

[34] J.I. Lee, F.D. Otto, A.E. Mathera, Equilibrium between carbon dioxide and aqueous monoethanolamine solutions, J. Chem. Technol. Biotechnol. 26 (1976) 541–549.

[35] E. Bender, U. Klein, W.Ph. Schmitt, J.M. Prausnitz, Thermodynamics of gas solubility: relation between equation-of-state and activity-coefficient models, Fluid Phase Equilib. 15 (1984) 241–255, https://doi.org/10.1016/0378-3812(84)87010-7.

[36] Y. Jou, J.J. Carroll, A.E. Mather, F.D. Otto, The solubility of nitrous oxide in water at high temperatures and pressures, Z. Phys. Chem. 177 (1992) 225–239, https://doi.org/10.1524/zpch.1992.177.Part_2.225.

[37] J.G.M.S. Monteiro, H.F. Svendsen, The N2O analogy in the CO2 capture context: literature review and thermodynamic modelling considerations, Chem. Eng. Sci. 126 (2015) 455–470, https://doi.org/10.1016/j.ces.2014.12.026.

[38] S.W. Brelvi, J.P. O'Connell, Corresponding states correlations for liquid compressibility and partial molal volumes of gases at infinite dilution in liquids, 18 (1972) 1239–1243, https://doi.org/10.1002/aic.690180622.

[39] S. Ali Mazari, T.H. Kang, S. Devkota, J.Y. Cha, B.J. Shin, J.H. Mun, K.M. Kim, U. Lee, J.H. Moon, Investigating the effect of blending of diamine and alkanolamine for CO2 capture: experiment and thermodynamic modeling of CO2-AEEA-DEA-H2O system, Chem. Eng. J. 470 (2023) 144141, https://doi.org/10.1016/j.cej.2023.144141.

[40] A. Benamor, M.K. Aroua, Modeling of CO2 solubility and carbamate concentration in DEA, MDEA and their mixtures using the Deshmukh-Mather model, Fluid Phase Equilib. 231 (2005) 150–162, https://doi.org/10.1016/j.fluid.2005.02.005.

[41] R. Deshmukh, A.E. Mather, A mathematical model for equilibrium solubility of hydrogen sulfide and carbon dioxide in aqueous alkanolamine solutions, Chem. Eng. Sci. 36 (1981) 355–362, https://doi.org/10.1016/0009-2509(81)85015-4.

[42] E.T. Hessen, T. Haug-Warberg, H.F. Svendsen, The refined e-NRTL model applied to CO2-H2O-alkanolamine systems, Chem. Eng. Sci. 65 (2010) 3638–3648, https://doi.org/10.1016/j.ces.2010.03.010.

[43] G.M. Bollas, C.C. Chen, P.I. Barton, Refined electrolyte-NRTL model: activity coefficient expressions for application to multi-electrolyte systems, AICHE J. 54 (2008) 1608–1624, https://doi.org/10.1002/aic.11485.

[44] L. Zong, C.C. Chen, Thermodynamic modeling of CO2 and H2S solubilities in aqueous DIPA solution, aqueous sulfolane-DIPA solution, and aqueous sulfolane-MDEA solution with electrolyte NRTL model, Fluid Phase Equilib. 306 (2011) 190–203, https://doi.org/10.1016/j.fluid.2011.04.007.

[45] W. Wagner, A. Pruss, International equations for the saturation properties of ordinary water substance. Revised according to the International Temperature

Scale of 1990. Addendum to J. Phys. Chem. Ref. data 16, 893 (1987), J. Phys. Chem. Ref. Data 22 (1993) 783–787, https://doi.org/10.1063/1.555926.
[46] I.M. Bernhardsen, H.K. Knuutila, Kinetics of CO2 absorption into aqueous solutions of 3-dimethylamino-1-propanol and 1-(2-hydroxyethyl)pyrrolidine in the blend with 3-(methylamino)propylamine, Chem. Eng. Sci.: X 3 (2019) 100032, https://doi.org/10.1016/j.cesx.2019.100032.
[47] I.M. Bernhardsen, L. Ansaloni, H.K. Betten, L. Deng, H.K. Knuutila, Effect of liquid viscosity on the performance of a non-porous membrane contactor for CO2 capture, Sep. Purif. Technol. 222 (2019) 188–201, https://doi.org/10.1016/j.seppur.2019.04.024.
[48] J.-J. Ko, M.-H. Li, Kinetics of absorption of carbon dioxide into solutions of n-methyldiethanolamine+water, Chem. Eng. Sci. 55 (2000) 4139–4147, https://doi.org/10.1016/S0009-2509(00)00079-8.
[49] E.B. Rinker, O.C. Sandall, Solubility of nitrous oxide in aqueous solutions of methyldiethanolamine, diethanolamine and mixtures of methyldiethanolamine and diethanolamine, Chem. Eng. Commun. 144 (1996) 85–94, https://doi.org/10.1080/00986449608936447.
[50] A. Hartono, O. Juliussen, H.F. Svendsen, Solubility of N2O in aqueous solution of diethylenetriamine, J. Chem. Eng. Data 53 (2008) 2696–2700, https://doi.org/10.1021/je800409d.
[51] A. Penttilä, C. Dell'Era, P. Uusi-Kyyny, V. Alopaeus, The henrys law constant of N2O and CO2 in aqueous binary and ternary amine solutions (MEA, DEA, DIPA, MDEA, and AMP), Fluid Phase Equilib. 311 (2011) 59–66, https://doi.org/10.1016/j.fluid.2011.08.019.
[52] M.A. Hamza, G. Serratrice, M.J. Stebe, J.J. Delpuech, Solute-solvent interactions in perfluorocarbon solutions of oxygen. An NMR study, J. Am. Chem. Soc. 103 (1981) 3733–3738, https://doi.org/10.1021/ja00403a020.
[53] J.J. Carroll, A.E. Mather, The system carbon dioxide-water and the Krichevsky-Kasarnovsky equation, J. Solution Chem. 21 (1992) 607–621, https://doi.org/10.1007/BF00650756.
[54] S.S. Laddha, J.M. Diaz, P.V. Danckwerts, The N2O analogy: The solubilities of CO2 and N2O in aqueous solutions of organic compounds, Chem. Eng. Sci. 36 (1981) 228–229, https://doi.org/10.1016/0009-2509(81)80074-7.
[55] B. Rumpf, G. Maurer, An experimental and theoretical investigation on the solubility of carbon dioxide in aqueous solutions of strong electrolytes, Ber. Bunsen. Phys. Chem 97 (1993) 85–97, https://doi.org/10.1002/bbpc.19930970116.
[56] G. Kontos, M.A. Soldatou, E. Tzimpilis, I. Tsivintzelis, Solubility of CO2in 2-Amino-2-methyl-1-propanol (AMP) and 3-(Methylamino)propylamine (MAPA): experimental investigation and modeling with the cubic-plus-association and the modified Kent-Eisenberg models, Separations 9 (2022) 338, https://doi.org/10.3390/separations9110338.
[57] M.W. Arshad, H.F. Svendsen, P.L. Fosbøl, N. Von Solms, K. Thomsen, Equilibrium total pressure and CO2 solubility in binary and ternary aqueous solutions of 2-(Diethylamino)ethanol (DEEA) and 3-(Methylamino)propylamine (MAPA), J. Chem. Eng. Data 59 (2014) 764–774, https://doi.org/10.1021/je400886w.
[58] N. El Hadri, D.V. Quang, E.L.V. Goetheer, M.R.M. Abu Zahra, Aqueous amine solution characterization for post-combustion CO2 capture process, Appl. Energy 185 (2017) 1433–1449, https://doi.org/10.1016/j.apenergy.2016.03.043.
[59] C. Tong, C.C. Perez, J. Chen, J.C.V. Marcos, T. Neveux, Y. Le Moullec, Measurement and calculation for CO2 solubility and kinetic rate in aqueous solutions of two tertiary amines, Energy Proc. 37 (2013) 2084–2093, https://doi.org/10.1016/j.egypro.2013.06.087. Elsevier Ltd.
[60] M. Xiao, H. Liu, H. Gao, Z. Liang, CO2 absorption with aqueous tertiary amine solutions: equilibrium solubility and thermodynamic modeling, J. Chem. Thermodyn. 122 (2018) 170–182, https://doi.org/10.1016/j.jct.2018.03.020.
[61] L. Dong, J. Chen, Y. Liu, J. Mi, Study on molecular structure of alkanolamines and their CO2 capture ability, Sci. Sin. Chim. 42 (2012) 291–296, https://doi.org/10.1360/032011-242.
[62] P. Brúder, A. Grimstvedt, T. Mejdell, H.F. Svendsen, CO2 capture into aqueous solutions of piperazine activated 2-amino-2-methyl-1-propanol, Chem. Eng. Sci. 66 (2011) 6193–6198, https://doi.org/10.1016/j.ces.2011.08.051.
[63] F. Meng, Y. Meng, T. Ju, S. Han, L. Lin, J. Jiang, Research progress of aqueous amine solution for CO2 capture: A review, Renew. Sustain. Energy Rev. 168 (2022) 112902, https://doi.org/10.1016/j.rser.2022.112902.
[64] I. Kim, H.F. Svendsen, Heat of absorption of carbon dioxide (CO2) in monoethanolamine (MEA) and 2-(aminoethyl)ethanolamine (AEEA) solutions, Ind. Eng. Chem. Res. 46 (2007) 5803–5809, https://doi.org/10.1021/ie0616489.
[65] H. Arcis, L. Rodier, K. Ballerat-Busserolles, J.Y. Coxam, Enthalpy of solution of CO2 in aqueous solutions of methyldiethanolamine at t = 372.9 k and pressures up to 5 MPa, J. Chem. Thermodyn. 41 (2009) 836–841, https://doi.org/10.1016/j.jct.2009.01.013.
[66] H. Kierzkowska-Pawlak, Enthalpies of absorption and solubility of CO2 in aqueous solutions of methyldiethanolamine, Sep. Sci. Technol. 42 (2007) 2723–2737, https://doi.org/10.1080/01496390701513032.
[67] F.A. Chowdhury, H. Okabe, H. Yamada, M. Onoda, Y. Fujioka, Synthesis and selection of hindered new amine absorbents for CO2 capture, Energy Proc. 4 (2011) 201–208. Elsevier Ltd, https://doi.org/10.1016/j.egypro.2011.01.042.
[68] H. Arcis, L. Rodier, J.Y. Coxam, Enthalpy of solution of CO2 in aqueous solutions of 2-amino-2-methyl-1-propanol, J. Chem. Thermodyn. 39 (2007) 878–887, https://doi.org/10.1016/j.jct.2006.11.011.